UiO : Department of Physics
University of Oslo

Computing the Phase Shift of $^1S_0$ Partial Wave of Nucleon-Nucleon Scattering

Erlend Lima

October 28, 2020

Abstract

Basic scattering theory is presented in an informal manner and used to derive two methods for computing the phase shift: by solving the integral equation of the K-matrix, and by solving the differential equation of the variable phase approach. The methods yield the same results, with the K-matrix being computationally less expensive. For the square well they agree with the analytical solutions. The Reid potential was used to model the $^1S_0$ partial wave of neutron-proton scattering. When compared to the experimental data of the Nijmegen group, the general shape is reproduced. The discrepancies are believed to be inherent to the Reid potential itself, not the methods used.

GitHub repository: https://github.com/ErlendLima/NuclearForces

Contents

1. Introduction

The interactions between nucleons are extremely complex and not yet fully understood. As the quarks and gluons dance together within nuclei, their strong interaction leaks out as the residual nuclear force, binding the nucleons together. In contrast to the electromagnetic force, the quantum field theory of the strong force does not allow itself for practical computation of the resulting nuclear force. As such, the nucleon-nucleon interaction must be described by approximations and phenomenological models.

The phase shift is a useful proxy for understanding nucleon-nucleon interaction, acting as a bridge between empirically obtained cross sections and theoretical models. Among these theoretical tools to compute the phase section are the *K-matrix theory* and the *variable phase approach*. Both of these are herein investigated by applying them to a proton-neutron system as well as the square well.

The methods are derived through the presentation of basic scattering theory. The scattering operator $\mathcal{S}$ and its relationship to the phase shift are introduced before moving on to informally deriving the Lippmann-Schwinger equations yielding the equation for the K-matrix. The regular solutions are then presented and used to derive the variable phase approach, Levinson's theorem, and explain several aspects of the phase shift.

The theory is written to be self-contained, with emphasis on the intuition instead of rigor. It mostly follows the excellent book of Taylor[1], but draws from multiple references. The numerical methods are implemented in the Julia language. All implementations as well as examples of their usage are available at https://github.com/ErlendLima/NuclearForces.

2. Theory

2.1. The Scattering Operator

Quantum scattering is a very complicated process, behaving so differently from the classical case of billiard balls that our intuition breaks down. Fortunately, the intricacies of the scattering process itself can be conveniently omitted by instead focusing on the relationship between the initial and resulting orbits. Specifically, the true orbit $|\psi\rangle$ is related to the asymptotic incoming and outgoing orbits $|\psi_{\text{in}}\rangle$ and $|\psi_{\text{out}}\rangle$ through the so-called *Møller operators* $\Omega_{\pm}$, defined as

$$\Omega_{\pm} = \lim_{t\to\infty} \mathcal{U}(t)^{\dagger}\mathcal{U}^{0}(t)$$

where $\mathcal{U}^{(0)}(t) = \exp\left[i\mathcal{H}^{(0)}t\right]$ are the familiar time evolution operators for the full and free Hamiltonians. We can then move between in true and asymptotic orbits with

$$\begin{aligned} |\psi\rangle &= \Omega_{+}\,|\psi_{\text{in}}\rangle \;\; = |\phi+\rangle \\ |\psi\rangle &= \Omega_{-}\,|\psi_{\text{out}}\rangle = |\phi-\rangle\,. \end{aligned}$$

If time dependence is added, the Møller operations allows one to move between the asymptotic orbits and the actual orbit at time t. Combining them, the outgoing orbit is related to the incoming orbit by

$$|\psi_{\text{out}}\rangle = \Omega_{-}^{\dagger}\Omega_{+}\,|\psi_{\text{in}}\rangle = \mathcal{S}\,|\psi_{\text{in}}\rangle$$

giving the definition of the *scattering operator* $\mathcal{S}$. Note that since the time evolution operator is unitary, and $\mathcal{S}$ is a product of time evolution operators, $\mathcal{S}$ is unitary. In the general case, let $|\chi-\rangle$ and $|\Phi+\rangle$ be any arbitrary orbits. The probability of the process $|\Phi+\rangle \to |\chi-\rangle$ occurring is then the square of the matrix element of $\mathcal{S}$:

$$w(\chi \leftarrow \Phi) = |\langle\chi-|\Phi+\rangle|^{2} = |\,\langle\chi|\mathcal{S}|\Phi\rangle|^{2}\,.$$

The probability w itself is not observable. Instead, what is measured is the related quantity *cross-section* $\sigma(\chi \leftarrow \Phi)$. The outgoing particle can scatter into a solid angle $d\Omega$, oriented in the direction of momentum $\vec{p}$. Likewise, the incoming particle can be described as wave packets with narrowly defined momentum $\vec{p_0}$. It can then be shown[1, p. 51] that the differential cross section is

$$\frac{\mathrm{d}\sigma}{\mathrm{d}\Omega} = |f(\vec{p} \leftarrow \vec{p_0})|^{2}$$

with $f(\vec{p} \leftarrow \vec{p_0})$ being the scattering amplitude, as known from elementary scattering theory. Note that only the magnitude of f can be obtained through the cross-section.

The next step is to relate the cross-section to the scattering operator. It can be shown[1, p. 40] that $\mathcal{S}$ commutes with the free Hamiltonian $\mathcal{H}^{0}$

$$\mathcal{H} = \mathcal{H}^{0} + V \qquad [\mathcal{H}^{0}, \mathcal{S}] = 0$$

Letting $|\mathbf{p}\rangle$ be the eigenvectors of $\mathcal{H}^0$ in momentum basis, we have for the scattering process $|p\rangle \to |p'\rangle$:

$$\langle \mathbf{p}'|[\mathcal{H}^0, \mathcal{S}]|\mathbf{p}\rangle = (E_{p'} - E_p)\langle \mathbf{p}'|\mathcal{S}|\mathbf{p}\rangle = 0$$

implying that $\langle \mathbf{p}'|\mathcal{S}|\mathbf{p}\rangle$ is zero except for $E_{p'} = E_p$. This leads to the form

$$\langle \mathbf{p}'|\mathcal{S}|\mathbf{p}\rangle = \delta(E_{p'} - E_p) \times \text{remainder}$$

where δ is the Dirac delta function.

At this point it is fruitful to define a new operator $\mathcal{R} \equiv 1 - \mathcal{S}$. $\mathcal{R}$ is the difference between the case of scattering and no scattering. It too commutes with $\mathcal{H}^0$, and so has the form

$$\langle \mathbf{p}'|\mathcal{R}|\mathbf{p}\rangle = -2\pi i \delta(E_{p'} - E_p) t(\mathbf{p}' \leftarrow \mathbf{p})$$

for some unknown function $t(\mathbf{p}' \leftarrow \mathbf{p})$ of p and p'. The factor $-2\pi i$ introduced to make future results more readable. The elements of $\mathcal{S}$ can therefore be written

$$\langle \mathbf{p}'|\mathcal{S}|\mathbf{p}\rangle = \delta(\mathbf{p}' - \mathbf{p}) - 2\pi i \delta(E_{p'} - E_p) t(\mathbf{p}' \leftarrow \mathbf{p}).$$

The function $t(\mathbf{p}' \leftarrow \mathbf{p})$ is continuous for most potentials and analytic for many[1, p. 42], but only defined for the "shell" $\mathbf{p}'^2 = \mathbf{p}^2$. However unphysical, it is beneficial to define an operator $\mathcal{T}$ whose matrix elements $\langle \mathbf{p}'|\mathcal{T}|\mathbf{p}\rangle$ are defined for all $\mathbf{p}$ and coincide with the values of t on the shell[a]. The matrix itself we denote T.

The scattering amplitude can be shown to be related to the on-shell T matrix elements as[1, p. 172]

$$f(\mathbf{p}' \leftarrow \mathbf{p}) = -(2\pi)^2 m t(\mathbf{p}' \leftarrow \mathbf{p}).$$

The elements of the scattering matrix can thus be written in terms of the scattering amplitude:

$$\langle \mathbf{p}'|\mathcal{S}|\mathbf{p}\rangle = \delta(\mathbf{p}' - \mathbf{p}) - \frac{i}{2\pi m}\delta(E_{p'} - E_p) f(\mathbf{p}' \leftarrow \mathbf{p}).$$

The first term describes the situation where no scattering occurs, while the second is the amplitude for when the wave is actually scattered, with the probability being the square of the scattering amplitude, hence its name.

2.2. Spherical Coordinates

The description of the scattering operators simplifies greatly when exploiting the spherical symmetry of many potentials. As known from elementary quantum mechanics, $\mathcal{H}^0$ commutes with the angular momentum operator $\mathcal{L}^2$ and z-axis projection $\mathcal{L}_3$. These three operators form a complete set of commuting observables. As $\mathcal{S}$ commutes with $\mathcal{H}^0$, $\mathcal{S}$ too commutes with the aforementioned operators, and is diagonal in the common basis, namely the basis of spherical waves $\{|Elm\rangle\}$, with E, $l(l+1)$ and m being the eigenvalues for $\mathcal{H}^0$,

[a] Note how there can not exist an operator $\tilde{\mathcal{T}}$ whose matrix *is* t, as the matrix must be defined *for all* p, p', not just the shell $p^2 = p'^2$.

$\mathcal{L}^2$ and $\mathcal{L}_3$ respectively. Since this basis diagonalizes $\mathcal{S}$, its matrix elements in this basis are

$$\langle E'l'm'|\mathcal{S}|Elm\rangle = \delta(E'-E)\delta_{l'l}\delta_{m'm}s_l(E).$$

$\mathcal{S}$ can be shown to be unitary, implying the eigenvalues $s_l(E)$ must have modulus one, justifying the form

$$\langle E'l'm'|\mathcal{S}|Elm\rangle = \delta(E'-E)\delta_{l'l}\delta_{m'm}\exp(2i\delta_l(E))$$

The quantity $\delta_l(E)$ is the important *phase shift*, an observable obtainable from both experiment and numerical calculations. It is purely real with an inherent ambiguity modulo π, as seen from

$$\exp(2i[\delta_l + n\pi]) = \exp(2i\delta_l)\exp(2in\pi) = \exp(2i\delta_l).$$

The decomposition of $f(\mathbf{p}' \leftarrow \mathbf{p})$ into partial waves can be obtained by exploiting the relation (dropping the subscripts for $E(p)$)

$$\langle \mathbf{p}'|(\mathcal{S}-1)|\mathbf{p}\rangle = \frac{i}{2\pi m}\delta(E'-E)f(\mathbf{p}' \leftarrow \mathbf{p}). \tag{2.1}$$

Inserting a complete set of states on the left hand side gives

$$\begin{aligned}
\langle \mathbf{p}'|(\mathcal{S}-1)|\mathbf{p}\rangle &= \int \mathrm{d}E \sum_{l,m} \langle \mathbf{p}'|(\mathcal{S}-1)|Elm\rangle \langle Elm|\mathbf{p}\rangle \\
&= \int \mathrm{d}E \sum_{l,m} (s_l(E)-1) \langle \mathbf{p}'|Elm\rangle \langle Elm|\mathbf{p}\rangle \\
&= \frac{1}{mp}\delta(E_{p'}-E_p)\sum_{l,m} Y_l^m(\hat{\mathrm{p}}')[s_l(E_p)-1]Y_l^m(\hat{\mathrm{p}})^*
\end{aligned}$$

where Y_l^m are the spherical harmonicals and the hât denotes unit vector. Combining this with (2.1), the amplitude can be decomposed into

$$f(\mathbf{p}' \leftarrow \mathbf{p}) = \frac{2\pi}{ip}\sum_{l,m} Y_l^m(\hat{\mathrm{p}}')[s_l(E_p)-1]Y_l^m(\hat{\mathrm{p}})^*$$

Letting $\hat{\mathrm{p}}$ lie along z and noting independence of m, we define

$$f(E_p,\theta) \equiv f(\mathbf{p}' \leftarrow \mathbf{p}) = \frac{1}{2ip}\sum_l (2l+1)[s_l(E_p)-1]P_l(\cos\theta).$$

This leads to the natural definition of the *partial wave amplitude* as

$$f_l(E) \equiv \frac{s_l(E)-1}{2ip} = \frac{\exp[2i\delta_l(\theta)]-1}{2ip} = \frac{\exp[2i\delta_l(E)]\sin\delta_l(E)}{p}.$$

Analogously the total cross-section can be decomposed into *partial wave cross-sections*, giving

$$\sigma(p) = \sum_l \sigma_l(p) = \sum_l 4\pi(2l+1)\left|f_l(p)\right|^2 = \sum_l 4\pi(2l+1)\frac{\sin^2\delta_l}{p^2}.$$

The magnitude of each partial wave cross-section is from this constrained by the so called *unitary bound*:

$$|\sigma_l| \leq 4\pi \frac{2l+1}{p^2}.$$

The maximal value is only reached if δ_l is an odd multiple of $\pi/2$.

General properties of the scattering process can be found by studying both the general and the limiting forms of the wave function. As before, the wave function of the full Hamiltonian $\langle \mathbf{x}|Elm+\rangle$ can be obtained from the wave function of the free Hamiltonian by the Møller operator

$$\langle \mathbf{x}|Elm+\rangle = \Omega_+ \langle \mathbf{x}|Elm\rangle ,$$

and hence we can get away with studying the free wave and transforming our results later. From basic quantum mechanics, we know it is on the form $\frac{1}{r}y(r)Y_l^m(\hat{\mathrm{x}})$ with $y(r)$ satisfying the radial Schrödinger equation

$$\left[\frac{\mathrm{d}^2}{\mathrm{d}r^2} - \frac{l(l+1)}{r^2} + p^2\right] y(r) = 0.$$

When $r \to 0$, $y(r)$ must go asr^{-l} or r^{l+1}. The latter condition is satisfied by the Riccati-Bessel functions $\hat{j}_l(z) = zj_l(z)$. Its limiting behavior as $z \to 0$ is

$$\hat{j}_l(z) \xrightarrow[z\to 0]{} \frac{z^{l+1}}{(2l+1)!!}\left[1 + \mathcal{O}(z^2)\right]. \tag{2.2}$$

The other limiting condition is satisfied by the Riccati-Neumann function $\hat{n}_l(z)$.

The wave function can therefore be written on the form

$$\langle \mathbf{x}|Elm\rangle = i^l \left(\frac{2m}{\pi p}\right)^{1/2} \frac{1}{r}\hat{j}^l(pr)Y_l^m(\hat{\mathrm{x}}). \tag{2.3}$$

On the other side, the limit $r \to \infty$ requires the boundary conditions $e^{\pm ipr}$. These are satisfied by the Riccati-Hankel functions $\hat{h}_l^{\pm}(z) = \hat{n}_l(z) \pm ij_l(z)$. Its limiting form is

$$\hat{h}_l^{\pm}(z) = e^{\pm i(z - l\pi/2)}\left[1 + \mathcal{O}(z^{-1})\right] \tag{2.4}$$

In analogy to (2.3), the full wave function can be written as

$$\langle \mathbf{x}|Elm+\rangle = i^l \left(\frac{2m}{\pi p}\right)^{1/2} \frac{1}{r}\psi_{lp}(r)Y_l^m(\hat{\mathrm{x}})$$

from which we see that $\psi_{lp}(r) \to \hat{j}_l(pr)$ when $V \to 0$. In the other limiting case $r \to \infty$, it can be shown [1, p. 187] to be

$$\psi_{lp}(r) \xrightarrow[r\to\infty]{} \frac{i}{2}\left[\hat{h}_l^-(pr) - s_l(p)\hat{h}_l^+(pr)\right] \tag{2.5}$$

or

$$\psi_{lp}(r) \xrightarrow[r\to\infty]{} \hat{j}_l(pr) + pf_l\hat{h}_l^+(pr).$$

Using the limiting forms (2.2) and (2.4) of the functions and some algebra, this can be rewritten as

$$\psi_{lp}(r) \xrightarrow[r\to\infty]{} e^{i\delta_l(p)} \sin\left[pr - \frac{1}{2}l\pi + \delta_l(p)\right].$$

This makes significance of the phase shift apparent. At large r the actual wave function becomes proportional to the free wave function

$$\hat{j}_l(pr) \to \sin\left(pr - \frac{1}{2}l\pi\right)$$

except that its oscillations are shifted by the phase shift δ_l.

2.3. Green's Function

One of the most important tools in scattering theory is *the resolvent*, or *Green's operator*. For many types of integral equations, a Green's function can be associated, transforming the solving of the equation to the computation of the Green's function. For our purposes the most important Green's operators are the *free Green's operator*

$$\mathcal{G}^0(z) \equiv (z - \mathcal{H}^0)^{-1}$$

and the *full Green's operator*

$$\mathcal{G}(z) \equiv (z - \mathcal{H})^{-1}$$

with $z \in \mathbb{C}$. The spectrum of $\mathcal{H}$ is discrete, with the orthonormal basis $|n\rangle$. The full Green's operator can then be written

$$\mathcal{G}(z) = (z - \mathcal{H})^{-1}1 = \sum_n \frac{|n\rangle\langle n|}{z - E_n}.$$

A specific matrix element is therefore

$$\langle\chi|\mathcal{G}(z)|\psi\rangle = \sum_n \frac{\langle\chi|n\rangle\,\langle n|\psi\rangle}{z - E_n}.$$

For any z not an eigenvalue E_n, the matrix element is well defined and analytic. When z is an eigenvalue, it is a simple pole with residue $\langle\chi|n\rangle\,\langle n|\psi\rangle$. That is, knowing the poles of $\mathcal{G}(z)$ gives information about the corresponding eigenvectors. As both the energy eigenvectors and eigenvalues can be found from $\mathcal{G}(z)$ itself, knowledge of $\mathcal{G}(z)$ is equivalent to solving the eigenvalue problem of $\mathcal{H}$[b]

While discrete spectra lead to poles in $\langle\chi|\mathcal{G}(z)|\psi\rangle$, continuous spectra lead to branch cuts. Consider the free Green's operator, which in terms of the angular momentum eigenvectors in analogy to the discrete spectrum has the matrix elements

$$\langle\chi|\mathcal{G}^0(z)|\psi\rangle = \int_0^\infty \frac{\mathrm{d}E}{z - E}\left\{\sum_{l,m}\langle\chi|Elm\rangle\,\langle Elm|\psi\rangle\right\}$$

[b] Of course, this is merely an intuitive explanation, not a proof. It can be shown that this is indeed true in the general case, see [1, p. 131].

that again gives well-defined functions for $z \notin \mathbb{R}^+$. For any $E^0 > 0$, the integral diverges. This can be seen by taking the difference between approaching the axis from the top and approaching it from the bottom, yielding[2, p. 469] $2\pi i \sum_{lm} |Elm\rangle\langle Elm|$.

The scattering process can yield both scattered states and bound states. The former is associated with continuous spectra while the latter with discrete. From the discussion above, scattered states correspond with branch cuts along $E^0 > 0$ while bound states show up as simple poles in $\mathcal{G}(z)$.

Finding $\mathcal{G}(z)$ is just as difficult as solving the eigenvalue problem for $\mathcal{H}$. Using $\mathcal{G}(z)$, however, yields an alternative numerical approach while at the same providing a powerful theoretical tool. The first step is to write $\mathcal{G}(z)$ in terms of the simpler $\mathcal{G}^0(z)$. This is trivially done using the algebraic relation

$$\mathcal{A}^{-1} = \mathcal{B}^{-1} + \mathcal{B}^{-1}(\mathcal{B} - \mathcal{A})\mathcal{A}^{-1}.$$

Inserting $\mathcal{A} = z - \mathcal{H}$ and $\mathcal{B} = z - \mathcal{H}^0$ gives

$$\mathcal{G}(z) = \mathcal{G}(z)^0 + \mathcal{G}(z)^0 V \mathcal{G}(z) = \mathcal{G}(z)^0 + \mathcal{G}(z) V \mathcal{G}(z)^0. \tag{2.6}$$

This is known as the *Lippmann-Schwinger equation for* $\mathcal{G}(z)$.

2.4. Lippman Schwinger

The Lippmann-Schwinger (LS) equation turns out to be a common and useful relation between operators in scattering theory. The derivation through Green's operators is not the historic path, and has the downside of obscuring its physical relationship to the Schrödinger equation. The benefit is its clear origins from a trivial algebraic relation, showing that there is not *the* LS equation, but many.

The operator $\mathcal{T}$ earlier introduced can be written as the potential plus the distortion to the potential caused by the full Green's operator[1, p. 137]:

$$\mathcal{T}(z) = V + V\mathcal{G}V. \tag{2.7}$$

It is clear that $\mathcal{T}(z)$ has the same properties as $\mathcal{G}(z)$ with respect to poles and branch cuts. Combining (2.7) with (2.6) together with some algebraic manipulations, we obtain the Lippmann-Schwinger equation for $\mathcal{T}(z)$:

$$\mathcal{T}(z) = V + V\mathcal{G}^0(z)\mathcal{T}(z). \tag{2.8}$$

In momentum space (2.8) is written as

$$\langle \mathbf{p}'|\mathcal{T}(z)|\mathbf{p}\rangle = \langle \mathbf{p}'|V|\mathbf{p}\rangle + \int \mathrm{d}^3p'' \frac{\langle \mathbf{p}|V|\mathbf{p}''\rangle}{z - E_{p''}} \langle \mathbf{p}''|\mathcal{T}(z)|\mathbf{p}\rangle$$

This highlights the need for introducing the $\mathcal{T}$ operator in the first place. There is no LS equation for the $\mathcal{S}$ operator because it requires the operators to be smooth functions, but $\mathcal{S}(z)$ is highly singular. On the other hand, $\mathcal{T}$ is analytic almost everywhere, allowing it to be expressed in terms of an integral equation.

Through a long and rather limit-finicky derivation, the $\mathcal{S}$ operator can be derived in terms of the $\mathcal{T}$ operator when z approaches the real axis from above

$$\langle \mathbf{p}'|S|\mathbf{p}\rangle = \delta(\mathbf{p}'-\mathbf{p}) - 2\pi i\delta(E_{p'}-E_p)\lim_{\epsilon\downarrow 0}\langle \mathbf{p}'|\mathcal{T}(E_p+i\epsilon)|\mathbf{p}\rangle\,.$$

This relation being the main motivation for defining $\mathcal{T}$ in the first place. It shows that $t(\mathbf{p}' \leftarrow \mathbf{p})$ corresponds to the on-shell T-matrix.

A reasonable question to ask is why computing the entire T-matrix is necessary when only the on-shell elements are physical. As already mentioned, one reason is computational. The on-shell elements are the limiting quantities of the off-shell elements. This doesn't mean that the off-shell elements are only a mathematical necessity. In fact, they correspond to the virtual interactions of the scattering process, which accounts for their fundamental unmeasurable nature. We are only allowed to observe the scattering in the non-interacting region, being the limiting case of the unobservable processes happening inside of the interacting region. Our initial starting point of focusing on the asymptotic states while ignoring the intricacies of the scattering is therefore not some mathematical trick to make computation easier, but an unavoidable requirement.

2.5. The K-Matrix

The Lippmann-Schwinger equation for $\mathcal{T}$ can not be solved by simple analytical methods. One recourse is to use approximation techniques. These are based on the expansion of $\mathcal{T}$ into the infinite sum[c]

$$\mathcal{T} = V + V\frac{1}{E-H^0+i\epsilon}V + V\frac{1}{E-H^0+i\epsilon}V\frac{1}{E-H^0+i\epsilon}V + \ldots$$

The unitarity condition of $\mathcal{T}$ is satisfied for the whole series, but violated for any finite order. If the series happens to be rapidly convergent, it may not pose a problem for numerical methods[d]. Nevertheless, a more stable approach is to enforce unitarity. The Caley transform achieves this, whereby a Hermitian operator is constructed in such a way as to ensure unitary.

The Caley transform of $\mathcal{S}$ is denoted by $\mathcal{K}$, and is defined as

$$\mathcal{K} = i\frac{1-\mathcal{S}}{1+\mathcal{S}}.$$

The K-matrix[e] is the matrix elements of the $\mathcal{K}$ operator:

$$\langle \mathbf{p}'|\mathcal{K}|\mathbf{p}\rangle = \delta(E_{p'}-E_p)k(\mathbf{p}' \leftarrow \mathbf{p}).$$

The advantage of $\mathcal{K}$ is that as long as it is Hermitian, $\mathcal{S}$, and by consequence $\mathcal{T}$, is guaranteed to be unitary. This property also holds for any Hermitian $\tilde{\mathcal{K}}$ that is not the true $\mathcal{K}$ of the scattering problem, for example due to numerical errors[5, 3].

[c] A lot of this section is based on [3] - a chapter from a book I've not been able to identify. It provides insights not stated as clearly elsewhere.

[d] That is to say, if the process described is sufficiently elastic, energy will be approximately conserved and convergence will be rapid. [4]

[e] The nomenclature of the K-matrix is a mess. It is also called the R-matrix, the T-matrix, the reaction matrix, the reactance matrix, the damping matrix, the distortion matrix, the dissipative matrix, and Heitler's matrix. To avoid overworking any of the other letters, I follow the style of Taylor.

From our definition of $\mathcal{R} = \mathcal{S} - 1$, the follows readily that

$$\mathcal{R} = 2i\mathcal{K} + i\mathcal{K}\mathcal{R}.$$

By taking the matrix elements we obtain the *Heitler's damping equation*

$$-\pi t(\mathbf{p}' \leftarrow \mathbf{p}) = k(\mathbf{p}' \leftarrow \mathbf{p}) - \pi i \int \mathrm{d}^3p\, k(\mathbf{p}' \leftarrow \mathbf{p}'')\delta(E_{p''} - E_p)t(\mathbf{p}'' \leftarrow \mathbf{p}).$$

The functions $t(\mathbf{p}' \leftarrow \mathbf{p})$ are as known the on-shell matrix elements of the $\mathcal{T}$ operator, and $\mathcal{T}$ has a related Lippmann-Schwinger equation (2.8). Heitler's damping equation allows us to substitute $\mathcal{K}$ for $\mathcal{T}$, giving the Lippmann-Schwinger equation for K[f]:

$$K = V + VP\mathcal{G}^0K \qquad *$$

where P denotes the principal value. The equivalent matrix element form for a central and spherically symmetric potential is[6]

$$\langle p'|K|p\rangle = \langle p'|V|p\rangle + \frac{2}{\pi}\int_0^\infty dp''\ \langle p'|V|p''\rangle\, \frac{1}{E - p''/m}\, \langle p''|K|p\rangle\,. \tag{2.9}*$$

This equation provides a numerically stable method to find the matrix K.

When $\mathcal{S}$ is symmetric, $\mathcal{K}$ is both Hermitian and symmetric, implying its matrix elements are real. As with $\mathcal{S}$ and $\mathcal{R}$, $\mathcal{K}$ becomes diagonal in the basis $\{|Elm\rangle\}$:

$$\begin{aligned}
\langle E'l'm'|\mathcal{S}|Elm\rangle &= \delta(E_{p'} - E_p)\delta_{l',l}\delta_{m',m}s_l(E)\\
\langle E'l'm'|\mathcal{R}|Elm\rangle &= \delta(E_{p'} - E_p)\delta_{l',l}\delta_{m',m}2ipf_l(E)\\
\langle E'l'm'|\mathcal{M}|Elm\rangle &= \delta(E_{p'} - E_p)\delta_{l',l}\delta_{m',m}k_l(E).
\end{aligned}$$

The elements $k_l(E)$ will in this case be real, and are directly related to the phase shifts:

$$k_l = i\frac{1 - s_l}{1 + s_l} = -\frac{1}{p}\tan\delta_l. \tag{2.10}*$$

That is, finding K by solving (2.9) lets us directly obtain the phase shift from the diagonal elements of K, and will be one of our two methods to compute the phase shift.

As a side note, the K-matrix is related standing wave stationary states in the same fashion that the T-matrix is related to plane wave stationary states. This is seen by writing the principal value of the Green's operator as

$$P\mathcal{G}^0 = P\frac{1}{E - \mathcal{H}^0} = \lim_{\varepsilon\to 0}\frac{1}{2}\left[\frac{1}{E - \mathcal{H}^0 + i\varepsilon} + \frac{1}{E - \mathcal{H}^0 - i\varepsilon}\right].$$

This is the Green's operator of an incoming wave and an outgoing wave, resulting in standing waves.

[f] The astute reader will notice that there are some factors $-i$, π and p missing. Their definitional absence makes results involving the reactance matrix more readable, but requires redefining $\mathcal{R}$ and $\mathcal{T}$, which in turn would make other results ugly. As the factors are ultimately irrelevant, I decided to ignore them and instead annotate the concerning equations with $*$. Compare e.g. [1, 6, 3] or any other reference for the total train wreck that otherwise ensues.

2.6. The Variable Phase Approach

An alternative way to compute the phase shift is through the variable phase approach (VPA). To develop it, it is useful to introduce another partial wave function $\phi_{lp}(r)$ that differs from $\psi_{lp}(r)$ only in its normalization. The VPA method is based on approximating the regular solution of a potential by the regular solution of a truncated potential. A differential equation is the result, the limit of which approaches the phase shift.

The regular solution is defined as the solution to the radial Schrödinger equation that behaves exactly as $\hat{j}_l$ as $r \to 0$:

$$\psi_{lp}(r) \xrightarrow[r\to 0]{} \hat{j}_l(pr).$$

Since both the boundary condition and the radial equation are real, $\psi_{lp}(r)$ is always real, hence the *regular* in its name. As different l yields different $\hat{j}_l(pr)$, different equations must be developed. We are only concerned with s-waves, and leave out the l-subscript. Define the truncated potential $V_\rho(r)$ by

$$V_\rho = \begin{cases} V(r) & r \leq \rho \\ 0 & r > \rho \end{cases}$$

The regular solution to the full potential is $\phi(r)$, while for the truncated potential it is $\phi_\rho(r)$. Likewise, the true phase shift is δ, and the phase shift for the truncated potential is $\delta(\rho)$. The inherent modulo π ambiguity in $\delta(\rho)$ is removed by defining $\delta(0) = 0$. As ρ increases, it is clear that the truncated potential approximates the true potential, hence

$$\delta(\rho) \xrightarrow[\rho\to\infty]{} \delta$$

For $r \leq \rho$, both regular solutions coincide[g]:

$$\phi(r) = \phi_\rho(r) \qquad r \leq \rho.$$

The truncated regular solution is given by

$$\phi_\rho(r) = \alpha(\rho) \sin\left[pr + \delta(\rho)\right],$$

for $\alpha(\rho)$ some coefficient. As $\phi_\rho(r)$ and $\phi(r)$ coincide for $r = \rho$, we have

$$\phi(\rho) = \alpha(\rho) \sin\left[p\rho + \delta(\rho)\right].$$

By same reasoning, the derivatives agree at the same point:

$$\dot{\phi}(\rho) = p\alpha(\rho) \cos\left[p\rho + \delta(\rho)\right].$$

The choice of ρ being arbitrary, the two relations hold for any ρ, and the variable can be substituted with r. Inserting them into the radial Schrödinger equation results in the VPA differential equation for s-waves:

$$\dot{\delta}(r) = -\frac{2m}{p} V(r) \sin^2[pr + \delta(r)]. \tag{2.11}$$

[g]Note the need for the *regular* solutions. The normalized solutions $\psi_{lp}(r)$ have different normalizations for different ρ, resulting in different values at r for different truncations.

Not only does the differential equation give the means to calculate the phase shift, it also gives some theoretical insights. The derivative of the phase shift is the potential V times some negative quantity $-\frac{2m}{p}\sin^2(\cdots)$. If the potential is purely negative, the derivative will be purely positive, and opposite for a purely positive potential. By definition $\delta(r=0)=0$, hence a negative potential yields a positive phase shift, and a positive potential yields a negative phase shift.

2.7. Levinson's Theorem

The regular solutions $\psi_{lp}(r)$ have already proved themselves as a useful tool in obtaining the phase shift numerically. It is however a gift that keeps on giving, and will now be used to derive[h] Levinson's theorem, stating that the phase shift in the limit $p \to 0$ equals the number of bound states n_l times π.

As $r \to \infty$, the regular solution must become proportional to the free solution, namely a combination of $\hat{h}_l^{\pm}$ with some suitable coefficients $\mathcal{J}_l(p)$:

$$\phi_{lp} \xrightarrow[r\to\infty]{} \frac{i}{2}\left[\mathcal{J}_l(p)\hat{h}_l^-(pr) - \mathcal{J}_l(p)^*\hat{h}_l^+(pr)\right]. \tag{2.12}$$

One of the asymptotic forms of the normalized solution is

$$\psi_{lp}(r) \xrightarrow[r\to\infty]{} \frac{i}{2}\left[\hat{h}_l^-(pr) - s_l(p)\hat{h}_l^+(pr)\right].$$

Comparing the two equations, we see that

$$s_l = \frac{\mathcal{J}_l(p)^*}{\mathcal{J}_l(p)},$$

and

$$\mathcal{J}_l(p) = \frac{\phi_{lp}(r)}{\psi_{lp}(r)}.$$

The coefficient function $\mathcal{J}_l(p)$ is hence the ratio of the two solutions. It proves to be a very important function, and is called the *Jost function*. It has an intimate relationship with the scattering matrix, having the same phase sign as s_l but opposite sign:

$$\mathcal{J}_l(p) = |\mathcal{J}_l(p)|\exp\{-i\delta_l(p)\}.$$

The Jost function is a function of the momentum, and to study its behavior, it is necessary to expand the momentum to become a complex variable. Although only real momenta are physical, the beauty of the complex plane opens up for physical insights.

The matrix elements s_l are meromorphic, i.e. analytic everywhere except at a finite number of points[i]. The poles in the upper and lower parts of the complex plane turn out to behave very differently, describing respectively bound states and resonances.

Restricting ourselves to the upper half plane, we can show that the poles of s_l indeed correspond to bound states. For most potentials the relation $\mathcal{J}_l(p)^* = \mathcal{J}_l(-p)$ holds. If the

[h] I say "derive". What follows is more of a proof sketch than a rigorous treatment, but will hopefully provide the intuition for the truth of the theorem.

[i] This is strictly only true for *nice* potentials. For our purposes we can pretend that all potentials are so nice. See [1, p. 220] for a more in-depth description.

Jost function vanishes for all $p \geq \bar{p}$, then we see from (2.12) that the regular solution will be an exponentially decreasing function above $\bar{p}$

$$\phi_{l\bar{p}} \xrightarrow[r\to\infty]{} -\frac{i}{2}\mathcal{J}_l(p)^*\hat{h}_l^+(pr).$$

As $\phi_{l\bar{p}}(r)$ vanishes at $r = 0$ by definition, it is in fact normalizable and hence a solution to the radial Schrödinger equation with energy $\frac{\bar{p}}{2m}$. The eigenvalues of the Hamiltonian are real, meaning $\bar{p}$ must be imaginary, $\bar{p} = i\alpha$. The point $\bar{p}$ is therefore a bound state with energy $\frac{-\alpha}{2m}$. The converse is also true[1, p. 224]. As $s_l(p) = \mathcal{J}_l(p)^*/\mathcal{J}_l(p)$, it follows that the when $\mathcal{J}_l(\bar{p}) = 0$, $s_l(\bar{p})$ is a simple pole having residue 1.

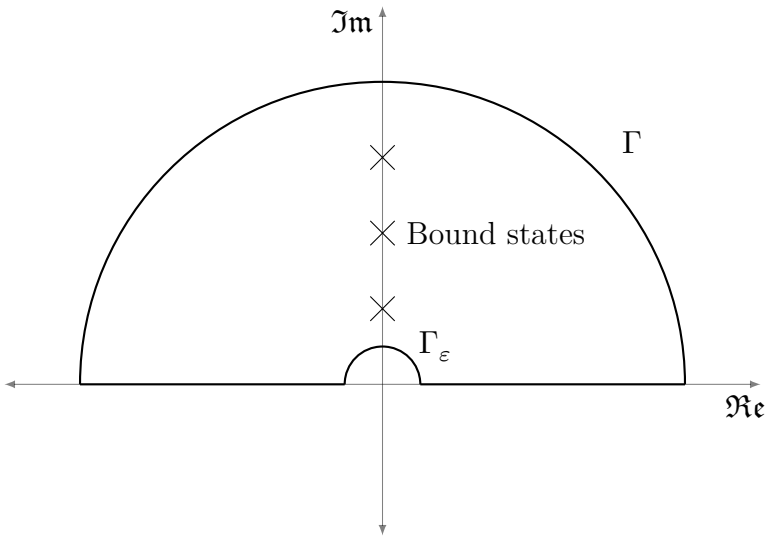

Figure 2.1: *The contour of integration. All of the poles of the integrand are contained within the contour. The radius of the larger semicircle is taken to infinity while the radius of the smaller is shrunk to zero. The crosses denote the simple poles, physically representing bound states.*

Levinson's theorem now follows from a simple integration. Consider the contour integral

$$I = \oint_\Gamma \mathrm{d}p \frac{\dot{\mathcal{J}}_l(p)}{\mathcal{J}_l(p)} = \oint_\Gamma \mathrm{d}p \ln \mathcal{J}_l(p)$$

where the contour Γ is half an annulus in the upper half plane. See Fig. 2.1. The integrand is analytic except at the n_l zeros of the Jost function, whence it has residue 1. By Cauchy's theorem

$$I = 2\pi i n_l.$$

When the radius of the larger semicircle is sufficiently large it will contain all of the finite poles, at which point on it has zero contribution. Letting the radius go to infinity, only the path along the real axis plus the smaller semicircle near 0 will contribute. On the positive real axis $\mathcal{J}_l(p) = |\mathcal{J}_l(p)| \exp\{-i\delta_l(p)\}$, so

$$\ln \mathcal{J}_l(p) = \ln |\mathcal{J}_l| - i\delta_l(p),$$

while on the negative real axis it is

$$\ln \mathcal{J}_l(-p) = \ln |\mathcal{J}_l| + i\delta_l(p).$$

The integral therefore evaluates to[j]

$$\begin{aligned} I &= \int_{-\infty}^{\infty} \mathrm{d}p \ln \mathcal{J}_l(p) + \oint_{\Gamma_\varepsilon} \mathrm{d}p \ln \mathcal{J}_l(p) \\ &= 2i[\delta_l(0) - \delta_l(\infty)] + \oint_{\Gamma_\varepsilon} \mathrm{d}p \ln \mathcal{J}_l(p) \end{aligned}$$

The small semicircle is a bit tricky to compute due to the Jost function's behavior near zero. With some rigorous treatment is can be coaxed into[1, p. 234]

$$\oint_{\Gamma_\varepsilon} \mathrm{d}p \ln \mathcal{J}_l(p) = \begin{cases} -\pi i & l = 0 \\ -2\pi i & l > 0 \end{cases}$$

Defining $\delta_l(\infty) = 0$ as before, we have for $l = 0$

$$\delta_l(0) = (n_0 + 1/2)\pi,$$

and for $l > 0$

$$\delta_l(0) = n_l \pi,$$

proving Levinson's theorem.

2.8. Resonances

Without delving into the fascinating subject of resonances, a quick word is in order to explain a phenomenon observed later. If $s_l(p)$ has a pole $\bar{p}$ in the lower half plane, and this pole is close to the real axis, then the phase shift can by approximated by the sum of a slowly changing component δ_{bg} and a rapidly changing component δ_{res}:

$$\delta_l(p) = \delta_{\text{bg}}(p) + \delta_{\text{res}}(p).$$

Such a point $\bar{p}$ causes a *resonance*. As $p \in \mathbb{R}$ moves from smaller to greater than the real part of $\bar{p}$, the component δ_{res} goes from 0 to π, causing an almost discontinuous jump in the phase shift. This manifests as a peak in the cross-section.

Resonances and bound states are closely related. If we increase the strength of the potential, the poles along the positive imaginary axis move up. If we decrease the strength, the poles move down. As the strength is further decreased, the poles eventually cross the origin and move along the imaginary axis. At this point the poles become resonances. An illustration is shown in Fig. 2.2. For $l > 0$, the poles can move along the entire lower plane, giving birth to other resonances for $p > 0$. For $l = 0$ the pole can only move along the imaginary axis, becoming more and more distant from the real axis, giving a weaker and weaker resonance. These are also called *virtual states* or *zero energy resonances*. Physically they represent metastable states, giving rise to a retarded scattered wave[1, p. 246].

[j] Strictly the contour path consists of the three pieces: $(-\infty, \epsilon)$, Γ_ε and (ε, ∞) along with appropriate limits. Consider this abuse of notation.

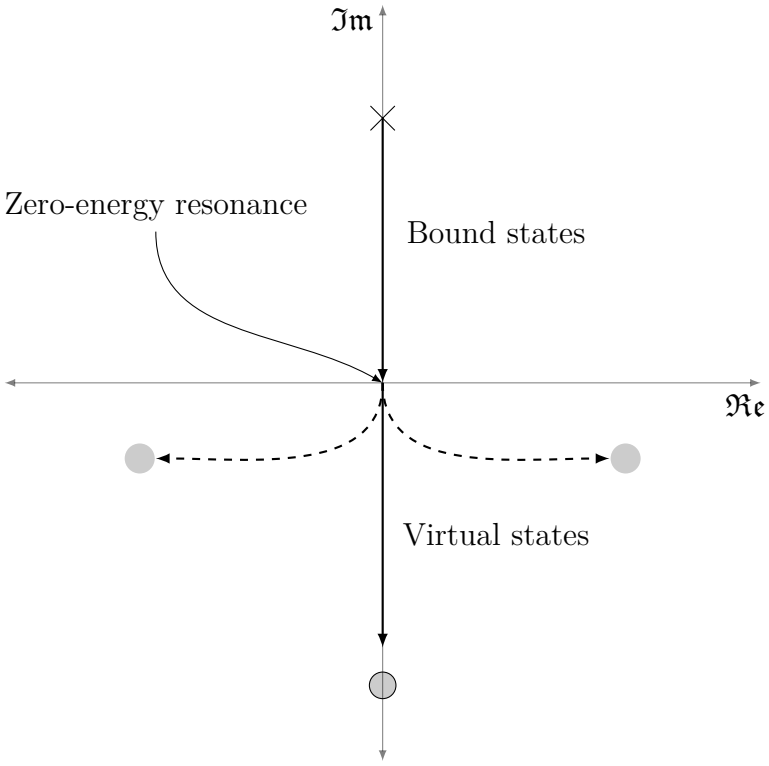

Figure 2.2: *The path of poles of $s_l(p)$ as a potential gets shallower. For s-waves the poles can only move along the imaginary axis, while higher waves can move along the entire lower plane (dashed arrows). The closer the poles are to the real axis, the greater the resonance. As the poles leave the imaginary axis, they split into n poles, where n is their residue.*

2.9. Potentials

2.9.1. The Square Well

Near and dear to everyone's heart is the square well potential; a simple discontinuous potential with value V_0 in the interacting region and zero everywhere else:

$$V(r) = \begin{cases} V_0 & \text{for } 0 \leq r \leq R \\ 0 & \text{for } r > R \end{cases}$$

The potential is plotted in Fig. 2.3

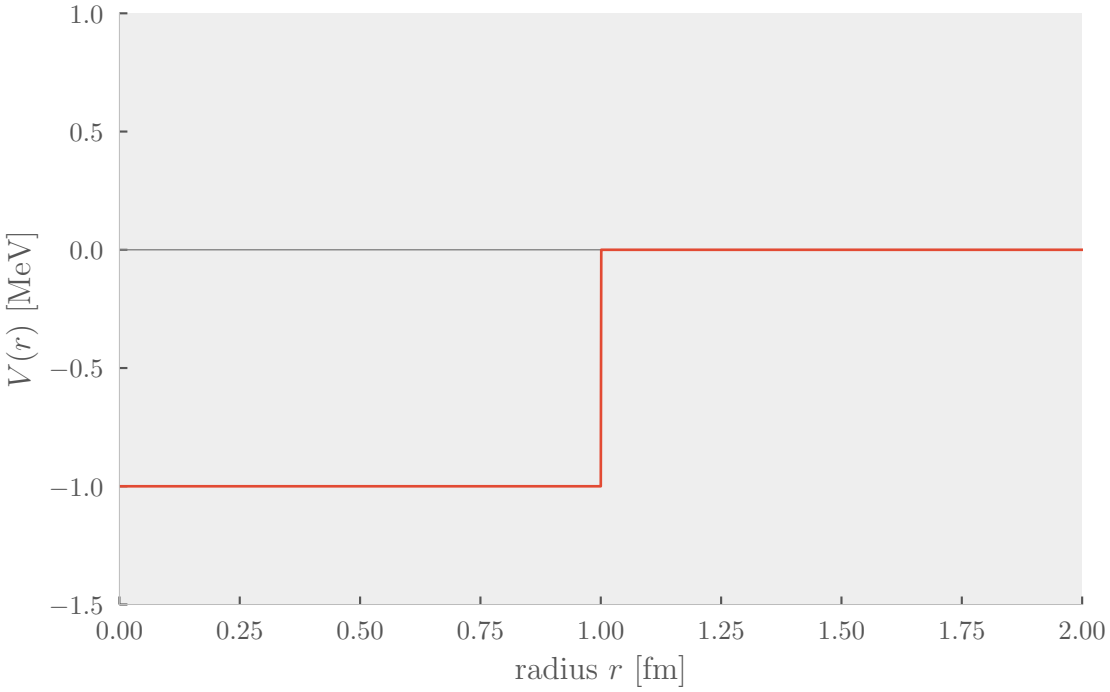

Figure 2.3: *An attractive square well potential with $V_0 = -1$ MeV.*

The analytic form of the phase shift for s-wave is[6]

$$\delta_0(E) = \arctan\sqrt{\frac{E}{E+V}} \cdot \tan\left(r\sqrt{2m(E+V)}\right) - r\sqrt{2mE}.$$

The disadvantage of this form is discontinuous jumps due to the phase shift's modulo π ambiguity. These can be smoothed out by

$$\delta_0(E) \equiv \operatorname{atan}\tan\delta_0(E)$$

2.9.2. The Yukawa Potential

In the 1930s there were several attempts at describing the nuclear force. Heisenberg considered the neutron to be composite of a proton and electron, an idea expanded on by Fermi into β-decay. Unable to explain the attractive forces holding the nucleus together, Yukawa modified their idea to let the mediating particle not be an electron or neutrino, but an yet unknown meson[7]. His prediction was proved right in 1947 with the discovery of the pion, yielding him the Nobel prize.

The potential Yukawa suggested was on the form

$$V(r) = -g^2\frac{e^{-\lambda r}}{r}$$

with a coupling constant g^2 related to the mass of the mediating boson. As it is entirely negative, it fails to account for the close range repulsive behavior observed in the nuclear force.

The Yukawa potential was later generalized into a class of *generalized Yukawa potentials*, potentials build on superpositions of Yukawa potentials:

$$V(r) = \sum_{i=1}^{N} C_i \frac{e^{-\eta_i r}}{r}$$

for some coefficients C_i and η_i.

A specific instance of a generalized Yukawa potential is the *Reid potential*[8]. It was an incremental improvement on already existing potentials at that time, building a parameterized potential where the exponent in each term reflects some phenomenological properties of the nuclear force while the constants are fit to phase shift data without consideration for their physical interpretation. In the case of proton-neutron scattering, the potential for the partial wave ${}^1S_0$ consists of the three terms:

$$V(r) = V_a \frac{e^{-ax}}{x} + V_b \frac{e^{-bx}}{x} + V_c \frac{e^{-cx}}{x}$$

where $x = \mu r$, $\mu = 0.7$ MeV, $V_a = -10.463$ MeV, $V_b = -1650.6$ MeV, $V_c = 6484.3$ MeV, and $a = 1$, $b = 4$ and $c = 7$.

The individual terms are plotted in Fig. 2.4 along with their sum. Its construction becomes apparent, where the three terms interact to form a strongly repulsive potential at close range along with an attractive well at a distance of about 1 fermi.

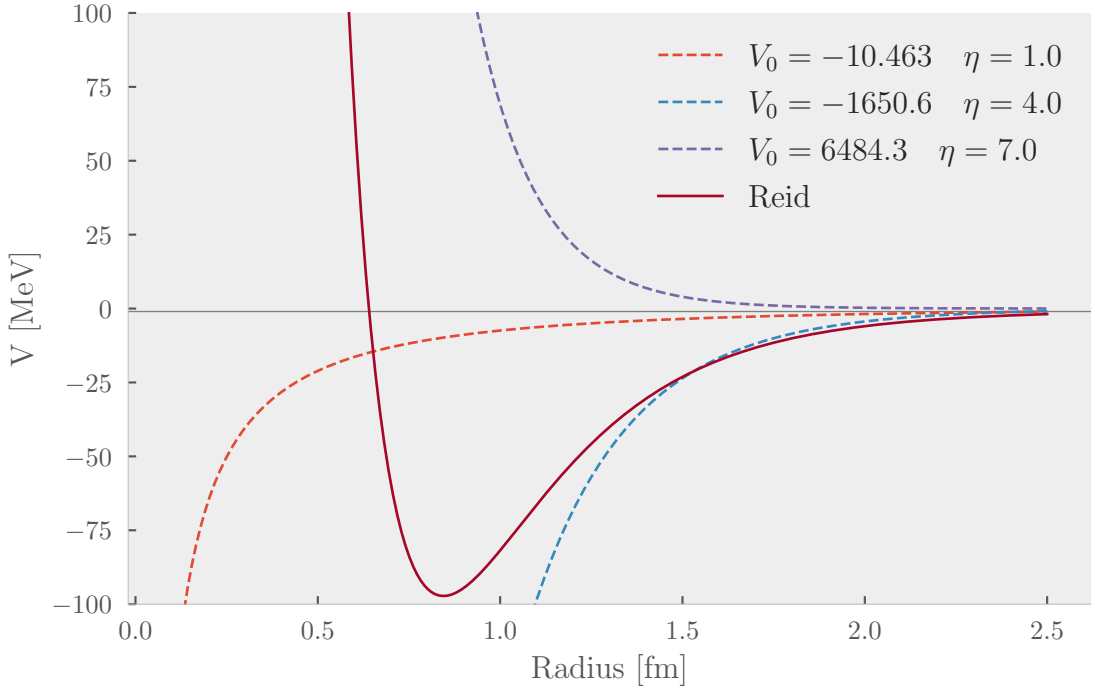

Figure 2.4: *The Reid potential (full stroke), a sum of three Yukawa potentials (dashed). It is has the typical characteristics of a nuclear force model, with a short range attractive potential followed by a repulsive core.*

The Reid potential for np ${}^1S_0$ was fit to several hundred data points of the phase shift in the region $0 - 350$ MeV, and thus should provide a good fit in this region[8].

2.9.3. Momentum Basis

Going from position to momentum space requires a change of basis, achieved through a Fourier transform. The problem is multidimensional, requiring a generalized Fourier transform. As we are only dealing with spherically symmetric and central potentials, the more suitable Hankel transform[k] can be used. For s-waves, it takes the form

$$\begin{aligned} V(k,k') &= \int_0^\infty j_0(kr)V(r)j_0(k'r)r^2\mathrm{d}r \\ &= \int_0^\infty \sin(kr)V(r)\sin(k'r)r^2\mathrm{d}r \end{aligned}$$

with the notation $V(k,k') = \langle k'|V|k\rangle$. The Yukawa potential in momentum basis is therefore

$$\begin{aligned} V(k,k') &= V_\eta \int_0^\infty j_0(kr)\frac{\exp(-\eta x)}{x}j_0(k'r)r^2\mathrm{d}r \\ &= \frac{V_\eta}{2\mu k k'}\int_0^\infty \mathrm{d}x\,(\cos\alpha x - \cos\beta x)\,\frac{\exp(-\eta x)}{x} \end{aligned}$$

with $\alpha = \frac{1}{\mu}(k-k')$ and $\beta = \frac{1}{\mu}(k-k')$. Adding and subtracting 1 lets us write the integral as

$$V(k,k') = \frac{V_\eta}{2\mu k k'}\left[\int_0^\infty \mathrm{d}x\,(1-\cos\beta x)\,\frac{\exp(-\eta x)}{x} - \int_0^\infty \mathrm{d}x\,(1-\cos\alpha x)\,\frac{\exp(-\eta x)}{x}\right]$$

Using a table of integrals we obtain our desired solution

$$V(k,k') = \frac{V_\eta}{\mu k k'}\ln\frac{(\mu\eta)^2+(k+k')^2}{(\mu\eta)^2+(k-k')^2}$$

The Reid potential in momentum basis is simply a sum of its terms in momentum basis.

[k] The Hankel transform can be regarded as the Fourier transform in hyperspherical coordinates, expanding the function in Bessel functions instead of sines and cosines.

3. Method

3.1. Discretizing Lippman-Schwinger

The equation (2.9) can be solved numerically by iteration, and is to this end discretized through a series of steps. The principal value poses a problem due to the limited precision of computers. To step around this, the integral is rewritten. The function $\frac{1}{k-k_0}$ is even about k_0, having equal parts of the curve above and below the x-axis, meaning

$$\int_{-\infty}^{\infty} \frac{\mathrm{d}k}{k-k_0} = 0.$$

Breaking the integral into its positive and negative parts and performing the substitution $k \to -k$ in the negative part then yields

$$\int_{0}^{\infty} \frac{\mathrm{d}k}{k^2-k_0^2} = 0.$$

The principal value can now be expressed as

$$\mathcal{P}\int_0^\infty \frac{f(k)}{k^2-k_0^2}\mathrm{d}k = \int_0^\infty \frac{f(k)-f(k_0)}{k^2-k_0}\mathrm{d}k$$

for $f(k)$ an arbitrary function. The integral is no longer singular at k_0, instead being proportional to $\frac{\mathrm{d}f}{\mathrm{d}k}$, allowing it to be computed numerically.

In particular, (2.9) can be recast to the form

$$K(k,k') = V(k,k') + \frac{2}{\pi}\int_0^\infty \mathrm{d}q \frac{q^2V(k,q)K(q,k'-k_0^2V(k,k_0)K(k_0,k')}{(k_0^2-q^2)/m}. \tag{3.1}$$

The integral is approximated through

$$\int_{-1}^{1} f(x)\mathrm{d}x \approx \sum_{i=1}^{N} f(x_i)w_i$$

for N lattice points through the corresponding weights w_i and points $x_i \in [-1,1]$. This is done through Gaussian-Legendre quadrature, using Legendre polynomials to construct the weights and corresponding points. To map the integral from $[-1,1]$ to $[0,\infty)$, the points and weights are transformed by

$$\begin{aligned} k_i &= C \times \tan\frac{\pi}{4}(1+x_i) \\ w_i &= C \times \frac{\pi}{4}\frac{w_i}{\cos^2\left(\frac{\pi}{4}(1-x_i)\right)} \end{aligned}$$

where C is a constant to fix the units.

Applied to our problem, (3.1) is discretized into

$$K(k,k') = V(k,k') + \frac{2}{\pi}\sum_{i=1}^{N}\frac{w_j k_j^2 V(k,k_j)K(k_j,k')}{(k_0^2-k_j^2)/m} - \frac{2}{\pi}k_0^2 V(k,k_0)K(k_0,k')\sum_{n=1}^{N}\frac{w_n}{(k_0^2-k_n^2)/m}.$$

There are $N\times N$ unknowns for $K(k,k')$, plus 1 for $K(k_0,k_0)$, for a total of $N+1$ unknowns. They can be described by a single extended K-matrix. Defining another matrix A as

$$A_{i,j} = \delta_{i,j} - V(k_i,k_j)u_k$$

with

$$u_j = \frac{2}{\pi}\frac{w_j k_j^2}{(k_0^2-k_j^2)/m} \qquad \text{for } j = 1,2,\ldots,N$$
$$u_{N+1} = -\frac{2}{\pi}\sum_{j=1}^{N}\frac{k_0^2 w_j}{(k_0^2-k_j^2)/m},$$

the equation can now be rendered as the matrix equation

$$AK = V.$$

Solving for K then simply amounts to inverting A and computing the product

$$K = A^{-1}V. \tag{3.2}$$

As known from (2.10), the diagonal of K is proportional to the phase shift

$$K(k_{N+1},k_{N+1}) = K(k_0,k_0) = -\frac{1}{mk_0}\tan\delta_0(k_0)$$

The matrix equation can be solved by standard matrix inversion methods available in the standard Julia library. The most time consuming part is the construction of the A-matrix. Its implementation is shown in Listing 1.

The number of mesh points N controls both the accuracy and the computational resources, demanding more memory and time as N increases. Running over the $(N+1)\times(N+1)$ matrices scales as roughly $\mathcal{O}(N+1)^2$ in both time and memory allocation. This is the expected behavior to compare to when measuring its actual resource usage.

3.2. Variable Phase Approach

In contrast to the LS approach, implementing the variable phase approach is straightforward. Julia has a very good differential equations solver DifferentialEq.jl[9], which is used for the actual computation. Since the limit in the relation $\delta(k) = \lim_{\rho\to\infty}\delta(k,\rho)$ can not be taken

Listing 1 The main loop of the K-matrix method.

```
function createA(V, k, ω, m)
    N = length(k)-1
    k₀ = k[end]
    A = diagm(0 => repeat([1.0,], N+1))
    uⱼ = 0.0

    @inbounds for j in 1:N+1
        uⱼ = 0.0
        if j ≠ N+1
            uⱼ = 2/π * ω[j]*k[j]^2/((k₀^2 - k[j]^2)/m)
        else
            for n in 1:N
                uⱼ += ω[n]*k₀^2/((k₀^2 - k[n]^2)/m)
            end
            uⱼ *= -2/π
        end

        for i in 1:N+1
            A[i, j] -= V[i, j] * uⱼ
        end
    end
    return A
end
```

Listing 2 Implementation of VPA in Julia

```
struct VPA <: Method
  rspan::Tuple{Float64, Float64}  # Range of the interaction
end
VPA() = VPA((1e-4, 15.0))


function (vpa::VPA)(k, m, V::Potential)
    function dδdr(δ, p, r)
      -1.0/k * 2.0m * V(r) * sin(k*r + δ)^2
    end

    δ0 = 0.0

    prob = ODEProblem(dδdr, δ0, vpa.rspan)
    sol = solve(prob, maxiters=10000, reltol=1e-8)

    δ = sol.u[end]
end
```

to infinity on a computer, ρ is instead substituted with a very large number, like 5. There is a trade-off between accuracy and computation time, with smaller ρ giving lesser accuracy while taking shorter time to compute, assuming the same step length is being used. To find the optimal ρ, several values were tried and the result compared to a high ρ.

The code implementation is shown in Listing 2

3.3. The Potentials

Two potentials are examined: the square well and the Reid potential. The former has analytical solutions and is relatively simple to understand, and will be used as a check on the implementation of the methods and to illustrate concepts discussed in the theory. The latter is more complicated, being a sum of three Yukawa potentials with the intent on modeling NN-interactions, with coefficients fitted to data.

Their precise implementations are not interesting, but are available in the file potentials.jl.

4. Results and Discussion

4.1. The Square Well Potential

The phase shift of the square well is found by VPA and compared to the analytical form. A well with the arbitrary depth of $V_0 = 4.0$ is used as example, with the computed curves shown in Fig. 4.1. The curves overlap, but the analytical solution has a jump at $k \approx 2.8$, stemming from the inherent modulo π ambiguity. The transformation $k \cot \delta$ lifts this ambiguity while fixing the phase shift to 0 at $k = 0$, plotted in the lower panel of the figure. Once transformed the curves overlap perfectly, as expected.

The simple form the square well potential allows us to illustrate some general behaviors of the phase shift. The phase shifts produced by several different well depths are plotted in Fig. 4.2 together with the corresponding cross sections in the lower panel. As $k \to 0$, all curves approach an integral multiple of π, and decrease towards zero as $k \to \infty$. As Levinson's theorem dictates, the multiple of π corresponds to the number of bound states each well can contain, with the number of states increasing as the potential deepens.

For some particular well depths, the cross-sections shoot up beyond the limits of the plot. The phase shift curves too have a characteristic shape, rising rapidly as they approach $k = 0$. Examples are marked by dashed lines. From our exposé on resonances in Section 2.8, we recognize these as zero energy resonances. Such curves indicate that the potential is on the verge of allowing for an additional bound state, producing a metastable state with cross-sections approaching the unitarity bound. Indeed, increasing the depth slightly makes the phase shift jump up to the next integral value.

A related phenomenon happens where the phase shift crosses $\delta = \pi$, at which point the cross-section falls off to zero. This is more clearly demonstrated in Fig. 4.3. A phase shift of $n\pi$ means the wave inside the well has precisely n more oscillations than the free wave. When the scattered wave exits the potential, it is exactly in phase with the free wave, and hence indistinguishable. If the higher $l > 0$ waves are negligible in the same region, the potential causes no scattering at all. This is the cause for the *Ramsauer-Townsend effect*[1, p. 195], where certain gases are completely transparent for electrons at a given energy.

For check that the method handles repulsive potentials, the phase shift is found for positive wells, see Fig. 4.4. We expect there to be no bound states, and for the phase shift to be negative. This is indeed the case, as the figure shows.

4.2. The Reid Potential

4.2.1. K-Matrix

The phase shifts for the ${}^1S_0$ partial wave of *np*-scattering obtained through the K-matrix method are shown in Fig. 4.5. This is compared to experimental data from the Nijmegen group, as well as their own pet model *nijm*93[10], also shown in the same figure. There is generally a good agreement, with all features of the experimental data being replicated; a rapid rise from 0 to $\approx 60°$, followed by a fall and a sign flip at ≈ 250 MeV. However, the computed phase shift is consistently lower than the experimental, and lower than *nijm*93 until the lines cross at 300 MeV.

The accuracy of the K-matrix calculations depends on the number of mesh points used. To determine its influence, different mesh sizes were used to compute the phase shift at the

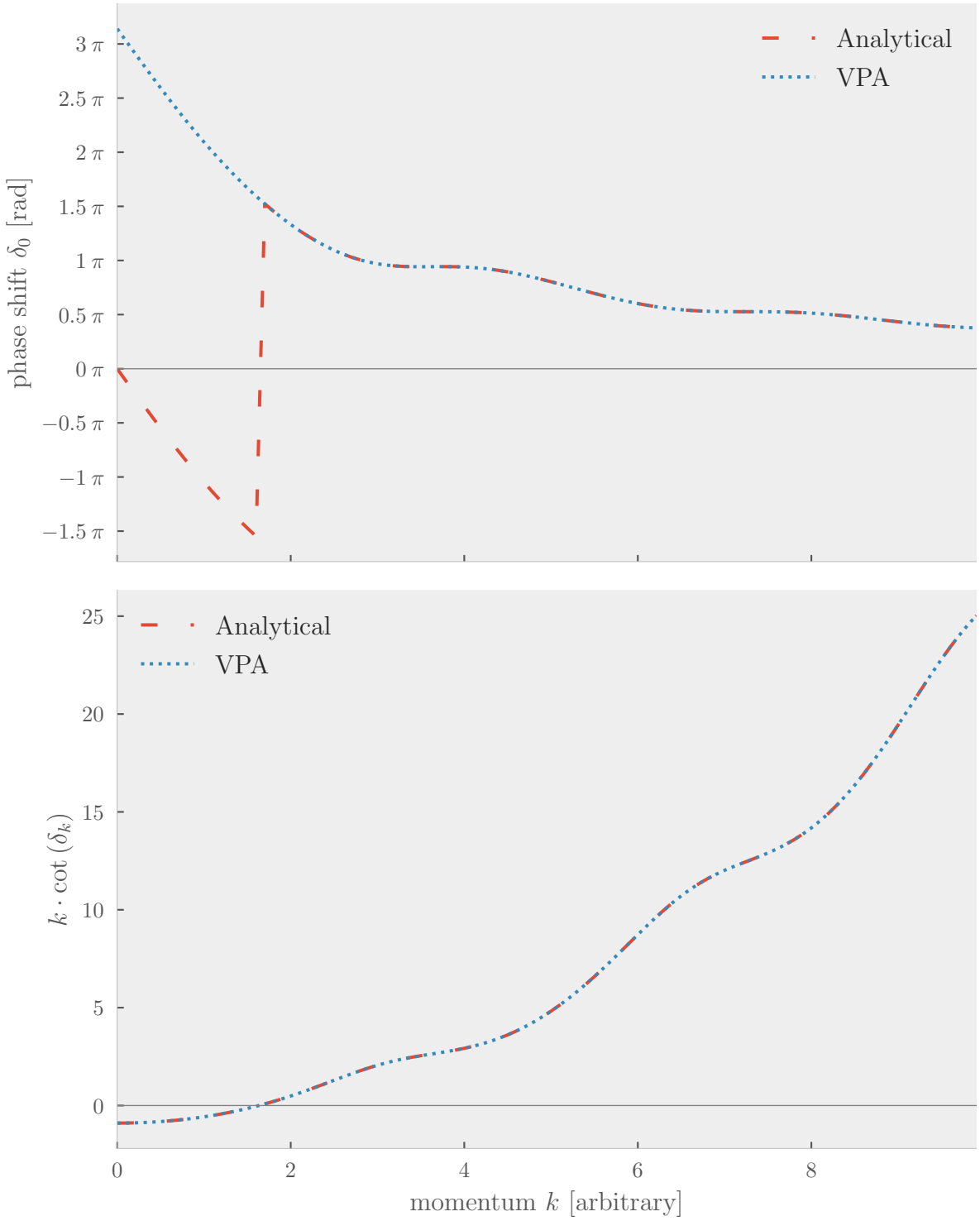

Figure 4.1: *The s-wave phase shift for a square well potential $V = -4$ MeV, and reduced mass of 1 MeV. The π-ambiguity in the analytical solution is lifted in the lower panel with the transformation $k \cot \delta_0$, showing a perfect overlap.*

same energies at the experimental data, and compared to them. The comparison was made by taking the total mean square error (MSE). See Fig. 4.6.

Unsurprisingly, the MSE starts off jumping before quickly falling off to a minimum at about 25 mesh points. As the MSE converges with just a few mesh points, the discrepancy ob-

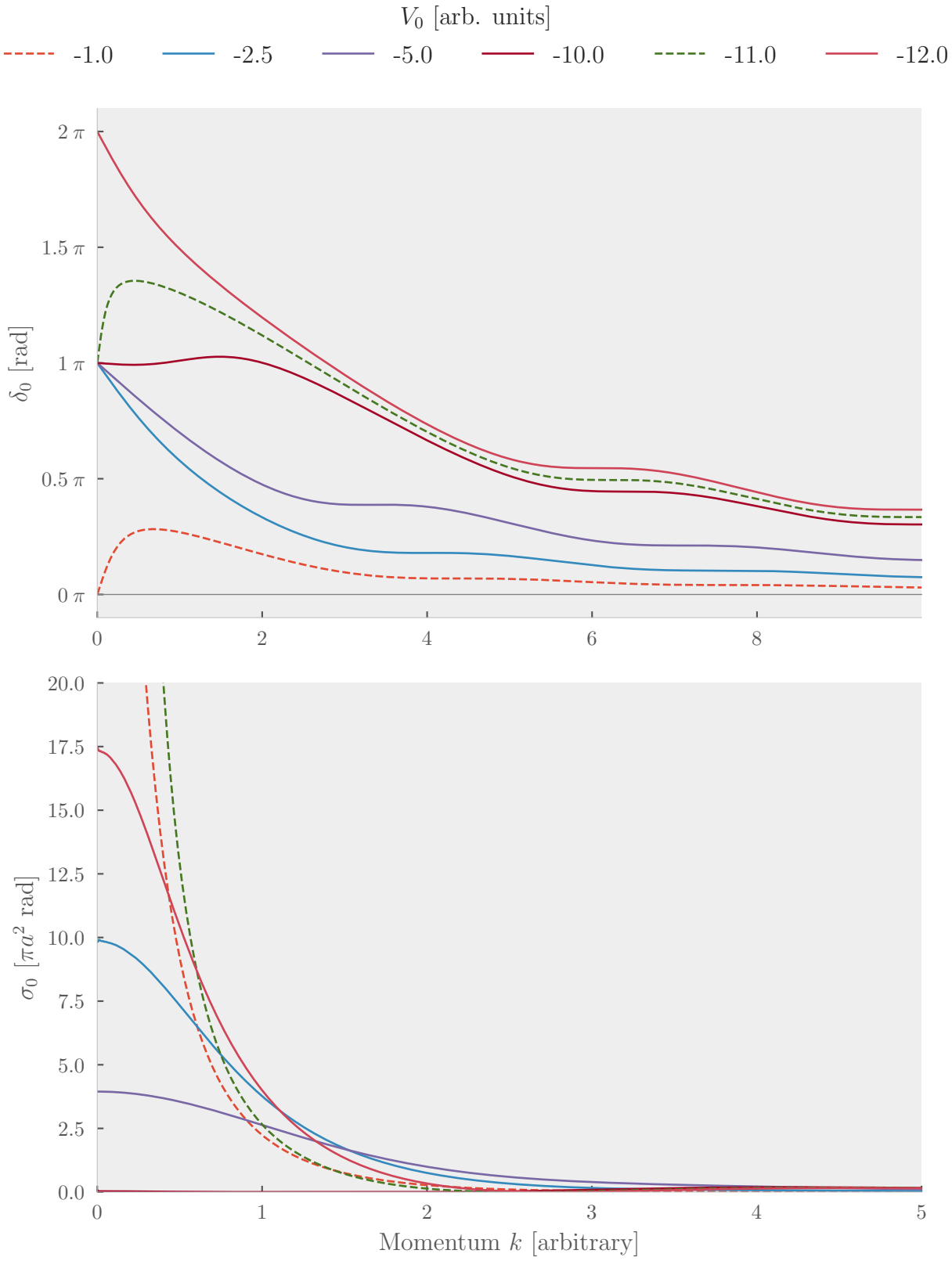

Figure 4.2: *The phase shift and corresponding cross section for several square wells of different depths. All curves fall off to zero by definition. As the wells deepen, the number of possible bound states increases, manifesting as curves starting at larger multiples of π. The dashed lines show the zero energy peaks.*

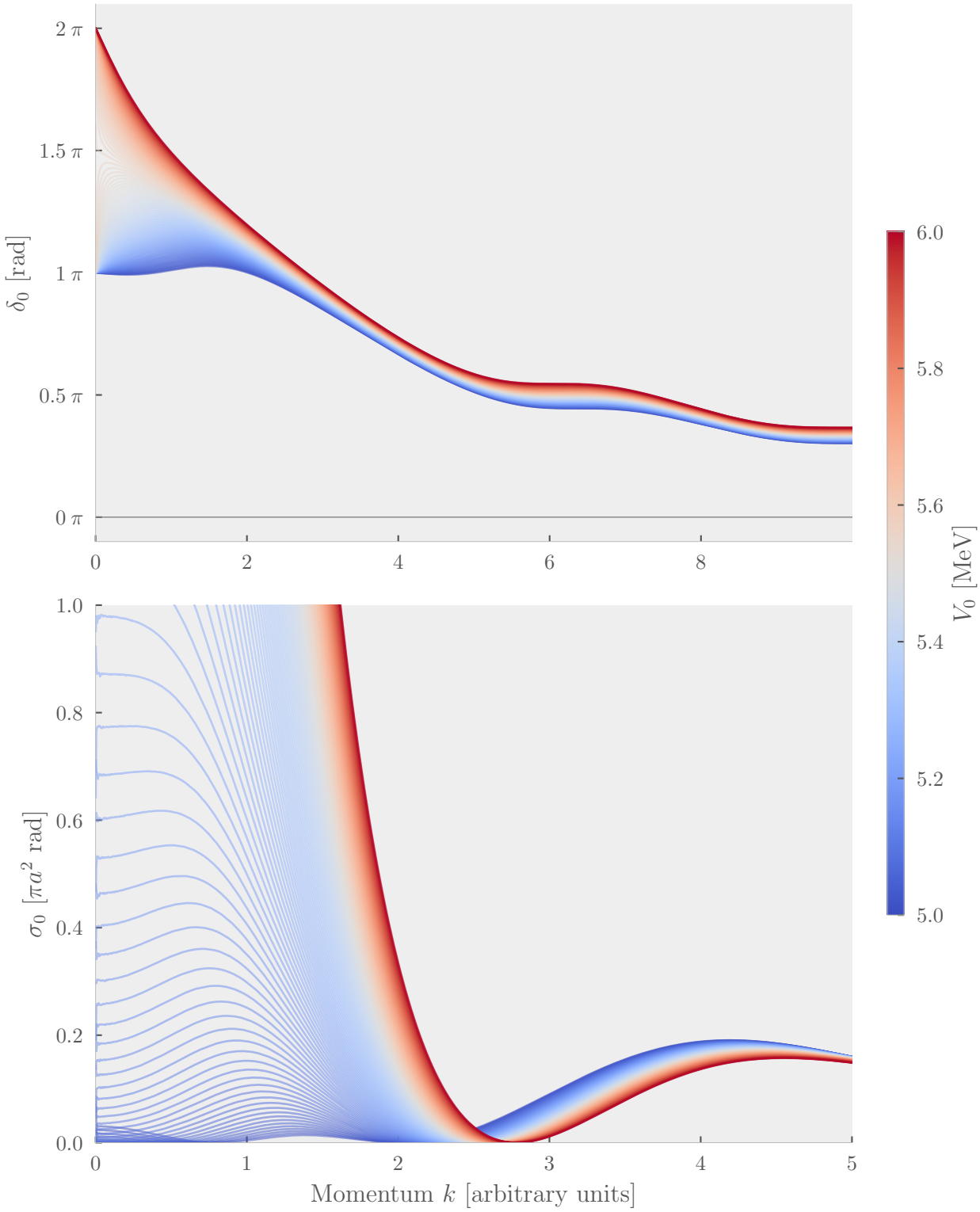

Figure 4.3: *Examples of phase shift curves crossing $\delta = \pi$. The scattered wave gets in phase with the free wave, ending up being equivalent with no scattering. The cross section plummets to zero when this happens.*

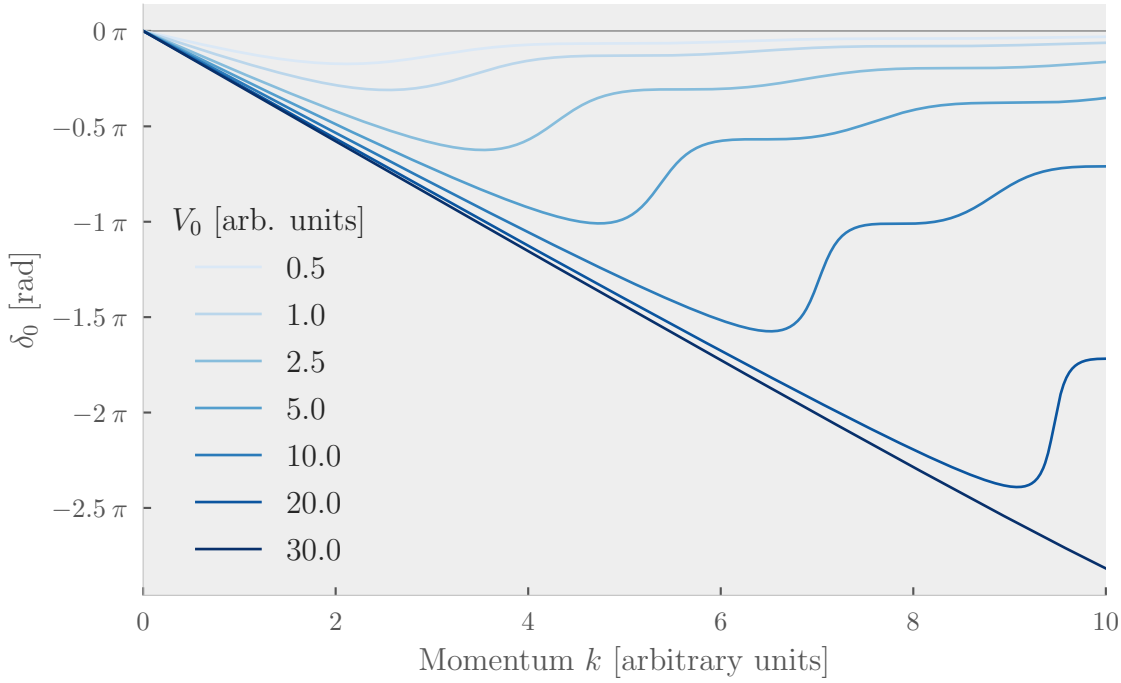

Figure 4.4: *The square well with positive well depths, yielding negative phase shifts and no bound states.*

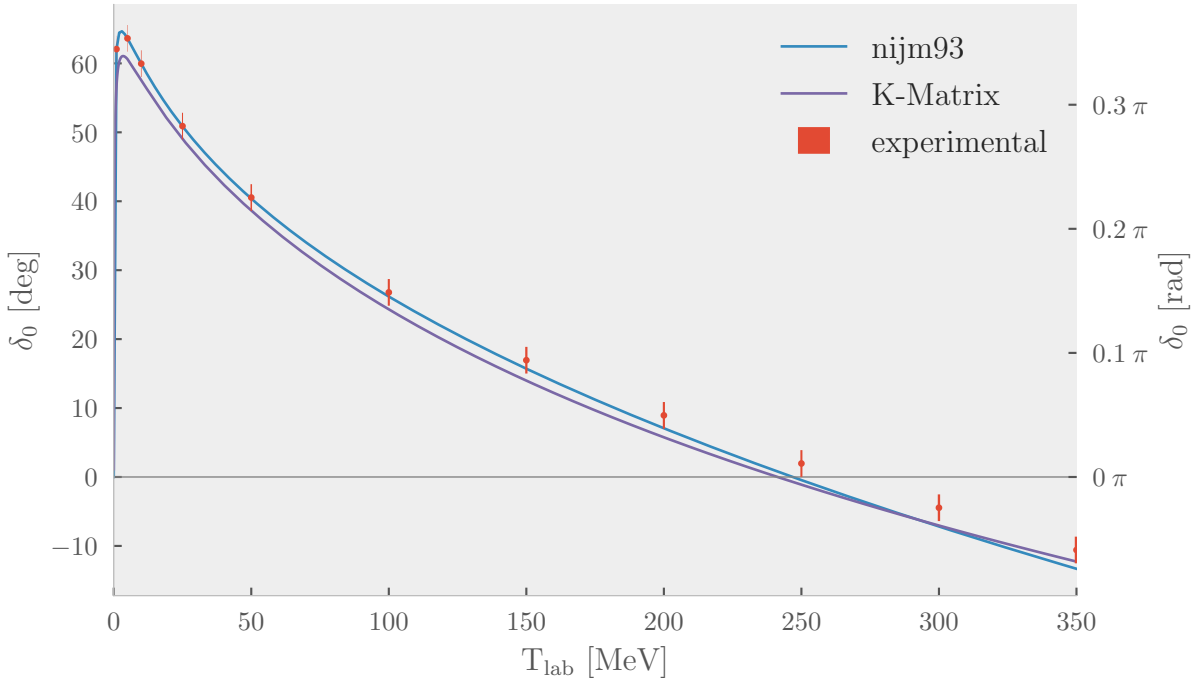

Figure 4.5: *Phase shift for* $^1S_0$ *partial wave of np-scattering found by K-matrix calculations using the Reid potential. The experimental data and nijm93 potential fit to aforementioned data are also shown, taken from[10] . There is good agreement, but the calculated phase shift is consistently lower than the experimental values. 30 mesh points were used in the calculation for each phase shift point.*

served in Fig. 4.5 can not be attributed to the method itself. Increasing the number further

gives negligible improvements. There is, however, an increasing cost in computational resources.

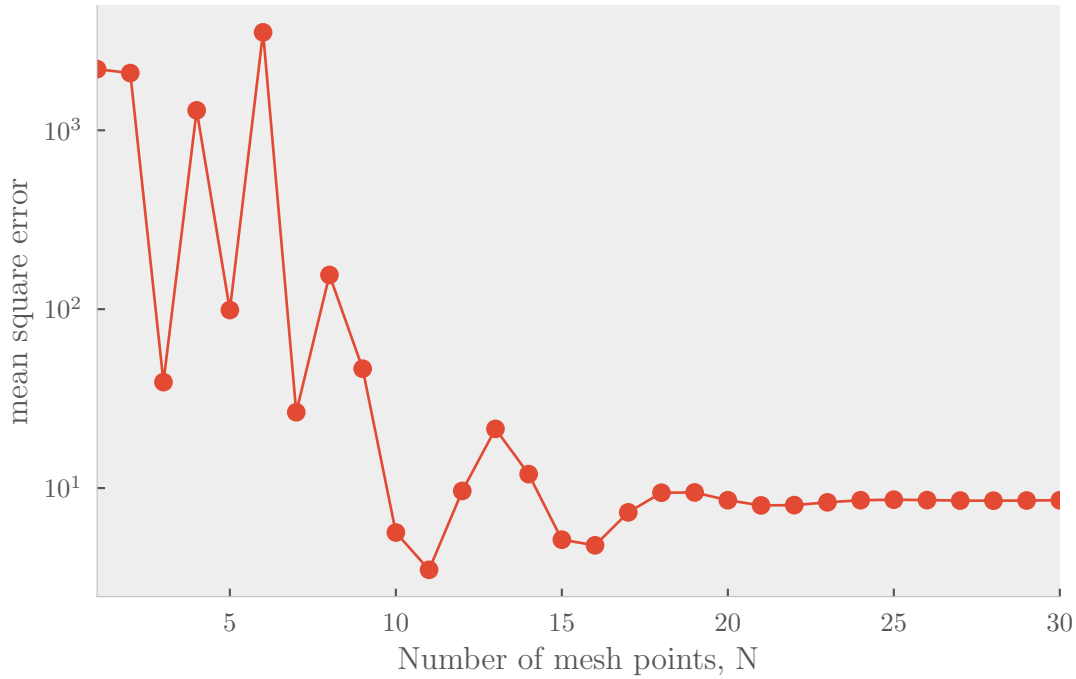

Figure 4.6: *The mean square error of the K-Matrix method as a function of number of mesh points. The computed values were compared to the mean of the experimental values. The For $n > 20$, the error remains near constant.*

The total computation time and amount of allocated bytes used by the K-matrix method is shown in Fig. 4.7. As discussed in Section 3.1, both the time and the memory is expected to increase by roughly $\mathcal{O}(N^2)$, N being the mesh size. Fitting second degree polynomials, we see that this is indeed roughly the case, with the required time being slightly chaotic due to the stochastic nature. The time was measured by repeating each calculation ten times and taking the median.

There is therefore a trade off between the resources required for a calculation and the accuracy obtained, a trade off that quickly gets increasingly poor, as no further benefit is obtained after ≈ 25 mesh points.

4.2.2. VPA

The second method for obtaining the phase shift from the Reid potential is the variable phase approach. As before, the results are compared with the Nijmegen results in Fig. 4.8, and not unexpectedly, it gives very similar results as Fig. 4.5.

VPA requires the cut-off[1] r_{end} of the potential to be sufficiently close to infinity to make the error negligible. Cutting off at low r_{end} can be computationally beneficial, so there is one more a trade off between accuracy and resource usage. The resulting phase shifts from different cut-off points are shown in Fig. 4.9. When the cut-off is too small, the potential is effectively a repulsive potential, yielding a negative phase shift. The phase shift gets

[1] I chose the notation r_{end} instead of the earlier used ρ to underline that ρ is a dummy variable for theoretical use, while r_{end} is a deliberate choice for when to stop the integration of the differential equation.

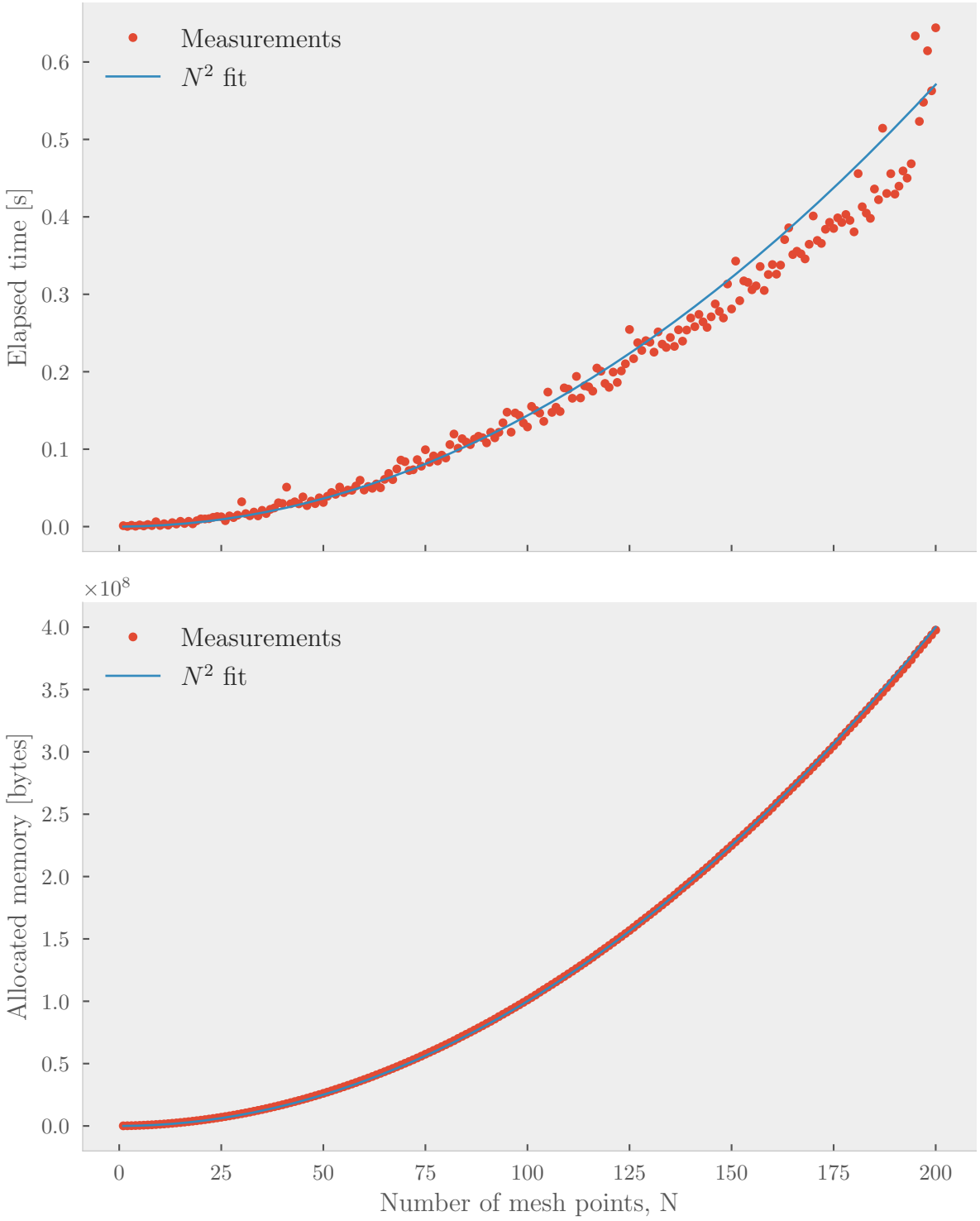

Figure 4.7: *Resource usage of the K-matrix method as a function of number of mesh points. The time shows the median of* 10 *repetitions.*

increasingly negative as the interaction "sees" more of the repulsive region, but once the attractive region is included, the phase shift quickly increases and converges to the far-away solution ($r_{\text{end}} = 15$).

The resource usage of VPA is significantly more difficult to measure, as the differential equation is solved by the external package DifferentialEq.jl, allowing for a range of different

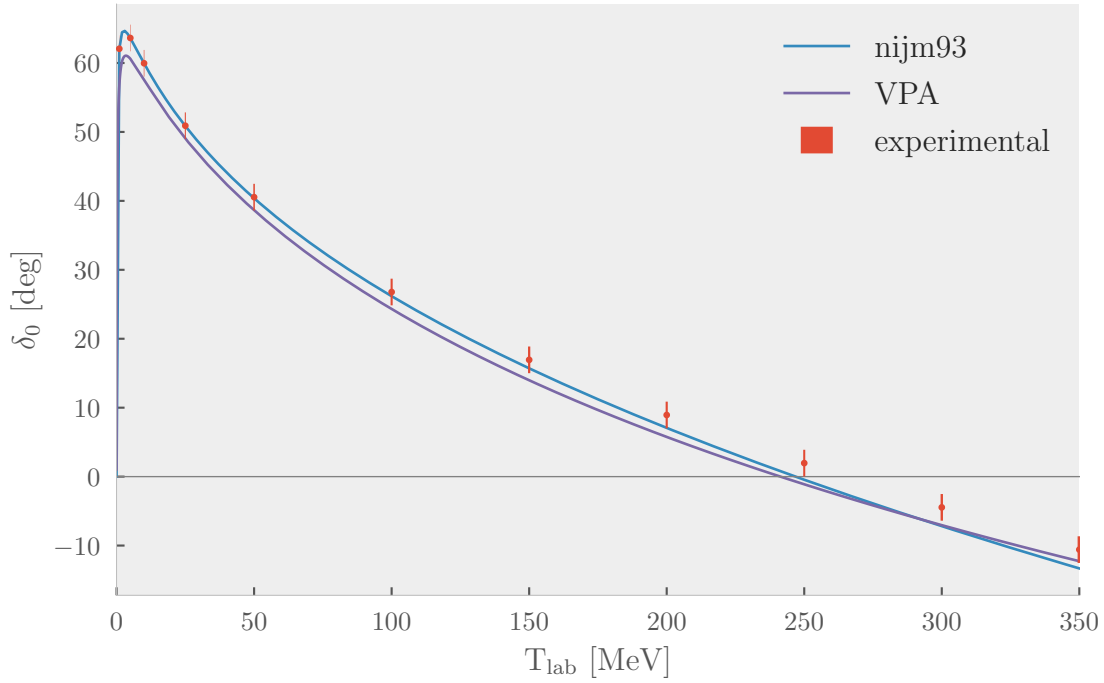

Figure 4.8: *The resulting s-wave phase shift from the variable phase approach alongside experimental Nijmegen data.*

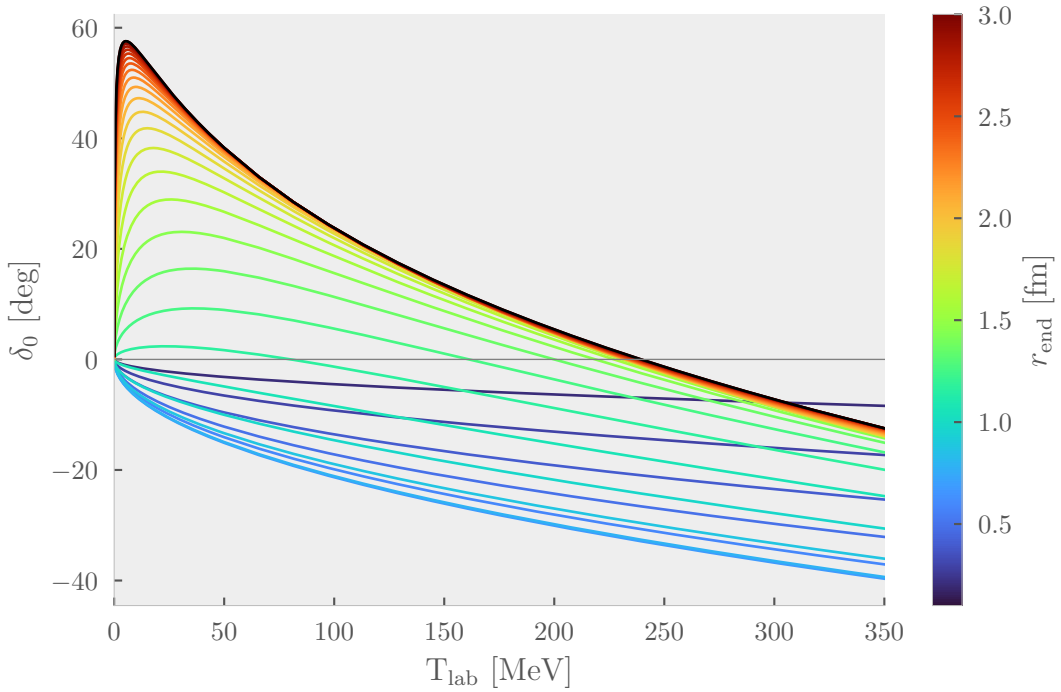

Figure 4.9: *The effect of using different cut off points r_{end} of the potential. Note how the different cut off points correspond to the different radii of Fig. 2.4.*

parameters and methods. For completeness' sake, the MSE, time and memory usage as a function of the step size are shown in the appendix Fig. A.1. The interesting information is that the time is nearly constant at ≈ 0.2 seconds for the same number of phase shift points

as the K-matrix method solved in Fig. 4.7. The K-matrix method is therefore significantly faster, with no loss in accuracy.

4.2.3. Comparison and Exploration

The phase shift from both K-matrix calculations and VPA are plotted together in Fig. 4.10 alongside the Nijmegen experimental data and their potential. The nijm93 potential was interpolated with linear interpolation to match up to the experimental data. The pointwise relative error is shown in the lower panel. Both curves obtained from the K-matrix method and VPA are perfectly overlapping, illustrating that they yield equivalent results of computing the phase shift. Since we already know that VPA is in agreement with the analytical solutions of the square well, we have confidence that the K-matrix method too is correctly implemented.

As the discrepancy between the theoretical computations and the experimental data can be attributed to neither the parameters of the methods nor the methods themselves, the culprit must be the model. The Reid potential was fitted to *np*-scattering data from the 60s and earlier. The later work of the Nijmegen group, as described in [10], used more data obtained through more accurate methods.

There are, however, some questions arising when examining the Nijmegen results. Their data was collected from a wide variety of sources, several of them through private communications. Although they have described their analysis in detail, some details are rather lacking, one of them being exactly whence the points shown in Fig. 4.10 originate. They do not seem to be experimental data per say, but rather a "representative sample" calculated from the experimental data. Their own *nijm*93 potential match these points well at lower energies, getting progressively worse as the energy increases. For $T_{\text{lab}} > 275$ MeV, the Reid potential yields better results. It is not at all clear whether the "experimental" data points should be held as the golden yardstick which the potentials ought to be compared.

The phase shift curve of the Reid potential has a striking resemblance to the dashed curves of Fig. 4.2. From our earlier discussion, it is easy to suspect there to be a bound state if the potential was just slightly more attractive. To examine this, the second term of the Reid potential was increased by a few percent, yielding the phase shift curves of Fig. 4.11. At $+3.37\%$ its strength, the phase shift at $k = 0$ jumps up to $180°$, allowing for a bound state by Levinson's theorem. This is a known experimental fact, the $T = 0$ singlet not having any bound state in contrast to the bound state of the $T = 1$ triplet, deuterium. It is striking, however, just how close the singlet is to obtaining a bound state.

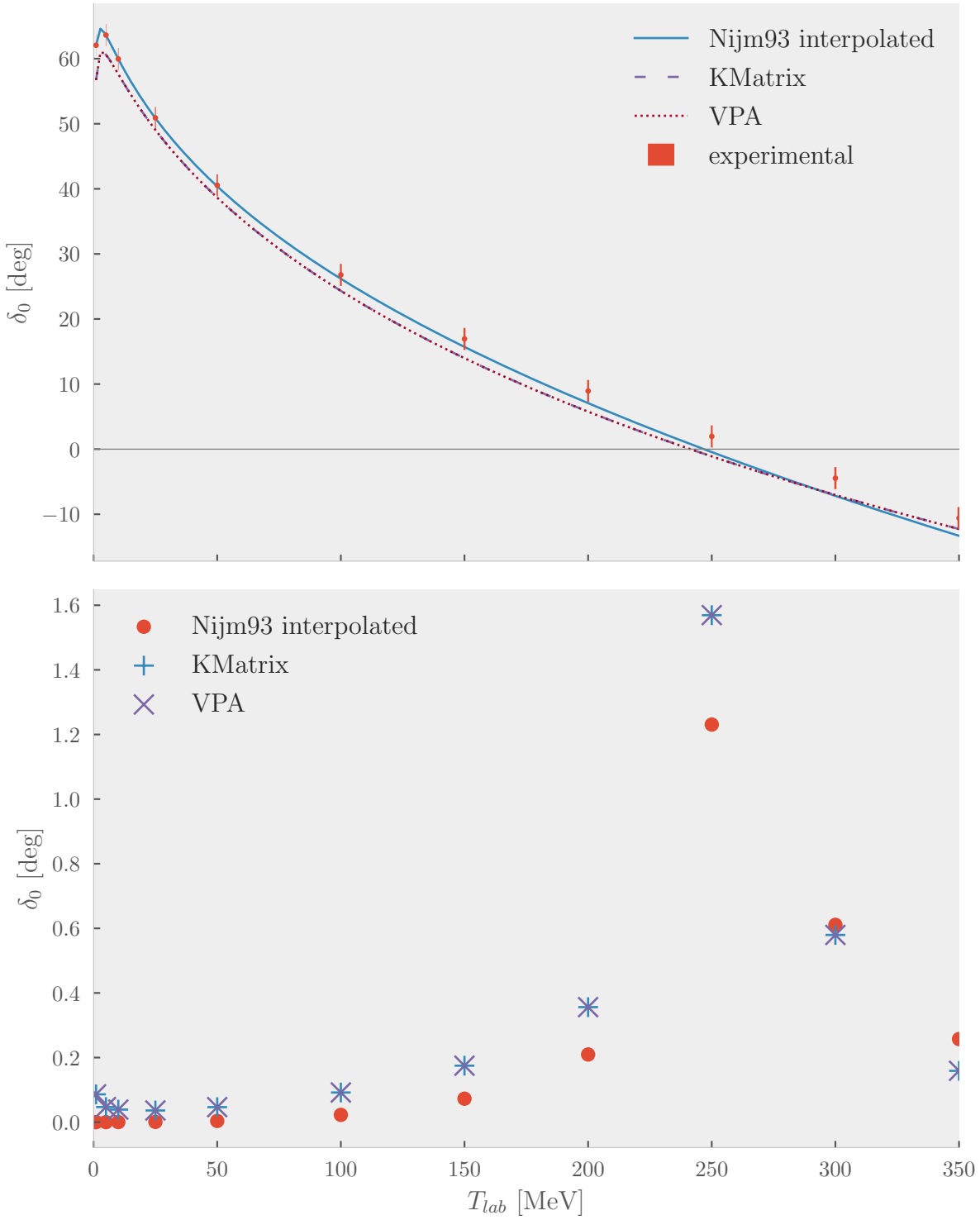

Figure 4.10: *The results of K-matrix and VPA using good parameters (mesh size of 30, r_{end} of 15, default diffeq-solver parameters), compared to the nijm93 data. The relative error is shown in the lower panel. Only $1 < T_{\text{lab}} < 100$ MeV are included; an arbitrary choice to exclude the jump at ≈ 0.1 MeV and the crossing near 250 MeV.*

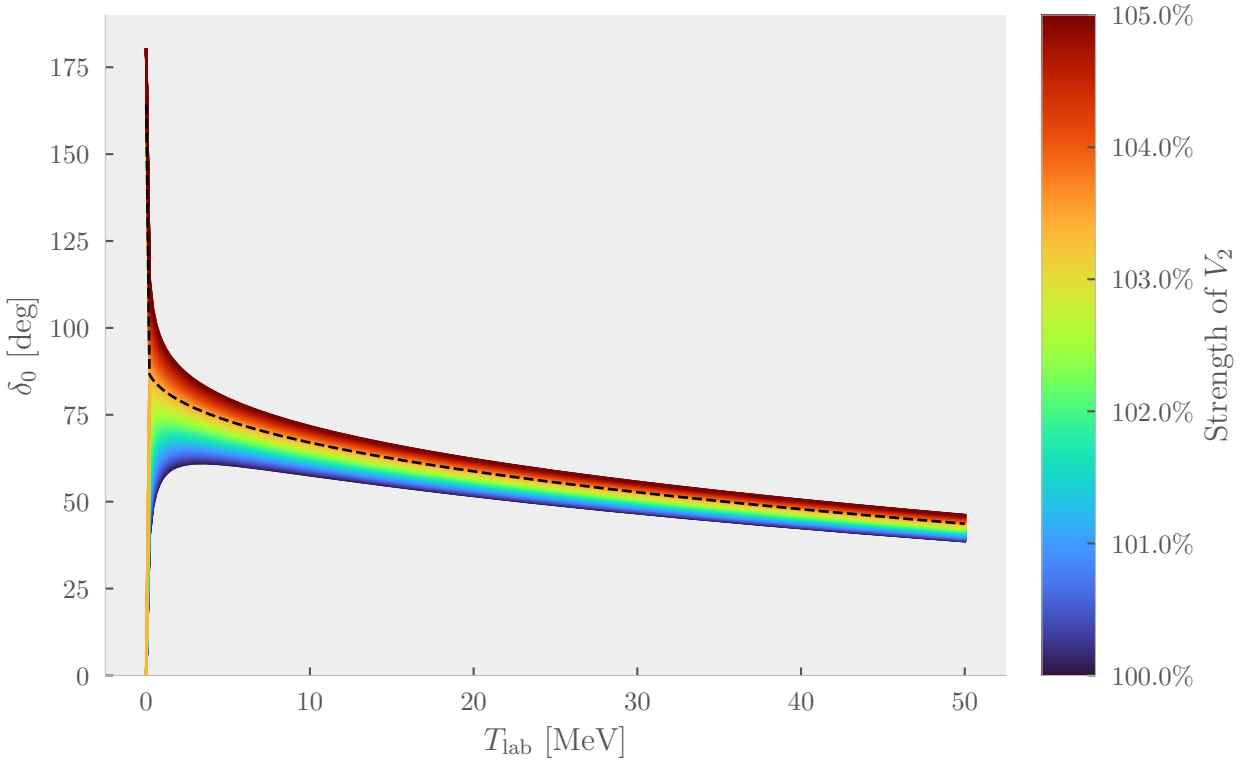

Figure 4.11: *The phase shift curves resulting from making the Reid potential more attractive by increasing the strength of its second term ($V_2 = -1650.6$ MeV). The initial blue 100% denotes its original value. At a 3.37% increase, the curves no longer begin at 0°, but jump to 180°. This is marked by a dashed line. The apparent lower start point is due to numerical inaccuracy.*

5. Conclusion

The basics of scattering theory was developed in terms of the $\mathcal{S}$ operator, yielding a plethora of fundamental results regarding the phase shift, K-matrix, bound states and Levinson's theorem. The theory gave birth to two methods for computing the phase shift: finding the K-matrix through its Lippmann-Schwinger equation, and solving the differential equation of the variable phase approach. They were used to find the phase shift of square wells and of the Reid potential modeling the s-wave scattering of a np system. Both methods gave equal phase shifts, with the phase shift of the square well matching the analytical solution. The phase shift of the Reid potential generally matched the experimental data of the Nijmegen group, but with discrepancies that can only be attributed to the Reid potential itself. Zero energy resonances were observed in square well examples as well as in the Reid potential, showing that the potential is on verge on allowing for a bound state.

References

[1] R. John Taylor. *Scattering Theory*. John Wiley & Sons, Inc., 1972 (cit. on pp. 1–3, 5–7, 9, 11–13, 21).

[2] Albert Messiah. *Quantum Mechanics*. John Wiley & Sons, Inc., 1961 (cit. on p. 7).

[3] Unknown. "Chapter 3 - Integral form of the Schrödinger equation". Excerpt from unknown book. Clearly explains the reasoning behind the reactance matrix. URL: http://shodhganga.inflibnet.ac.in/bitstream/10603/68621/9/09_chapter%5C%203.pdf (cit. on pp. 8, 9).

[4] Eric C. Le Ru, Walter R. C. Somerville, and Baptiste Auguié. "Radiative correction in approximate treatments of electromagnetic scattering by point and body scatterers". In: *Physical Review A* 87.1 (Jan. 2013). DOI: 10.1103/physreva.87.012504. URL: https://doi.org/10.1103%2Fphysreva.87.012504 (cit. on p. 8).

[5] Laszlo Szunyogh. "Introduction to Multiple Scattering Theory". Short text obtained through the web. URL: http://newton.phy.bme.hu/~szunyogh/Elszerk/Kkr-slides.pdf (cit. on p. 8).

[6] (Cit. on pp. 9, 15).

[7] Hideki Yukawa. "On the Interaction of Elementary Particles. I". In: *Progress of Theoretical Physics Supplement* 1 (Jan. 1955), pp. 1–10. ISSN: 0375-9687. DOI: 10.1143/PTPS.1.1. eprint: https://academic.oup.com/ptps/article-pdf/doi/10.1143/PTPS.1.1/5310694/1-1.pdf. URL: https://doi.org/10.1143/PTPS.1.1 (cit. on p. 15).

[8] Roderick V Reid. "Local phenomenological nucleon-nucleon potentials". In: *Annals of Physics* 50.3 (1968), pp. 411–448. ISSN: 0003-4916. DOI: https://doi.org/10.1016/0003-4916(68)90126-7. URL: http://www.sciencedirect.com/science/article/pii/0003491668901267 (cit. on p. 16).

[9] Christopher Rackauckas and Qing Nie. "Differentialequations.jl–a performant and feature-rich ecosystem for solving differential equations in julia". In: *Journal of Open Research Software* 5.1 (2017) (cit. on p. 19).

[10] V. G. J. Stoks et al. "Partial-wave analysis of all nucleon-nucleon scattering data below 350 MeV". In: *Phys. Rev. C* 48 (2 Aug. 1993), pp. 792–815. DOI: 10.1103/PhysRevC.48.792. URL: https://link.aps.org/doi/10.1103/PhysRevC.48.792 (cit. on pp. 21, 25, 29).

Appendices

A. VPA Resource usage

The resource usage of VPA by varying the step size of the solver, Fig. A.1.

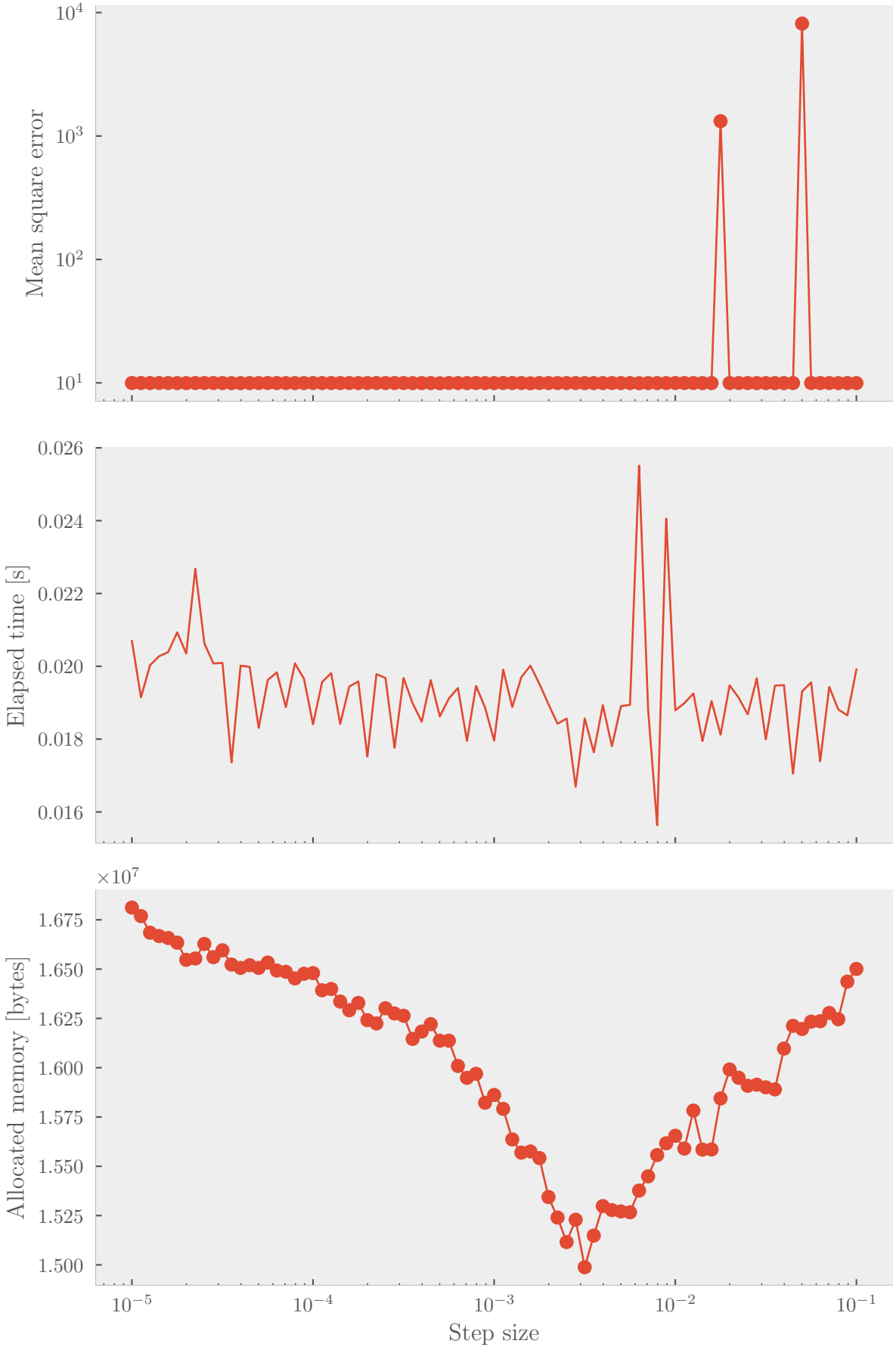

Figure A.1: *Mean square error and resource usage of VPA as a function of step size of the solver. Only allocated memory has a significant change, reaching a minimum at* 0.008